AD-A085 035 ILLINOIS UNIV AT URBANA-CHAMPAIGN COORDINATED SCIENCE LAB F/G 20/1
THEORY OF GUIDED ACOUSTIC WAVES IN PIEZOELECTRIC SOLIDS.(U)
JUL 79 S DATTA DAAG29-78-C-0016
UNCLASSIFIED R-849 NL

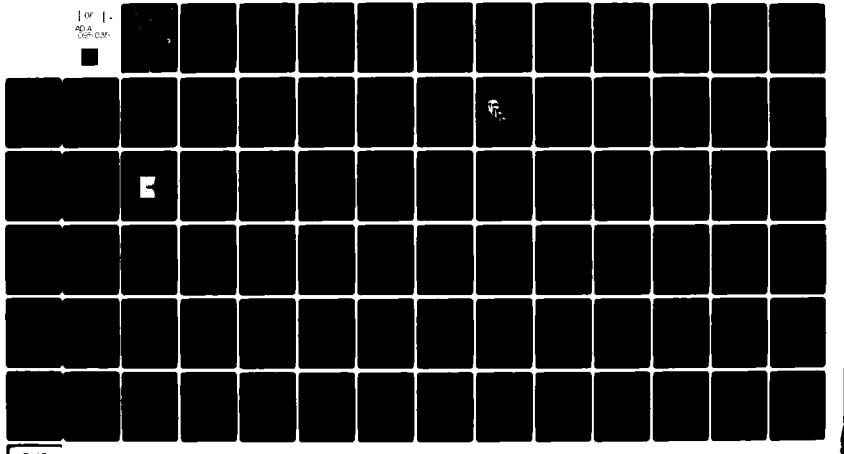

END
DATE FILMED
7-80
DTIC

REPORT R-849 JULY, 1979 UILU-ENG 78-2242

CSL COORDINATED SCIENCE LABORATORY

THEORY OF GUIDED ACOUSTIC WAVES IN PIEZOELECTRIC SOLIDS

SUPRIYO DATTA

UNIVERSITY OF ILLINOIS - URBANA, ILLINOIS

UNCLASSIFIED

SECURITY CLASSIFICATION OF THIS PAGE (When Data Entered)

REPORT DOCUMENTATION PAGE	READ INSTRUCTIONS BEFORE COMPLETING FORM
1. REPORT NUMBER	2. GOVT ACCESSION NO. 3. RECIPIENT'S CATALOG NUMBER
4. TITLE (and Subtitle) THEORY OF GUIDED ACOUSTIC WAVES IN PIEZOELECTRIC SOLIDS.	5. TYPE OF REPORT & PERIOD COVERED Technical Report
	6. PERFORMING ORG. REPORT NUMBER R-849, UILU-ENG-78-2242
7. AUTHOR(s) Supriyo Datta	8. CONTRACT OR GRANT NUMBER(s) DAAG29-78-C-0016; N00014-79-C-0424; F19623-78-C-0040
9. PERFORMING ORGANIZATION NAME AND ADDRESS Coordinated Science Laboratory University of Illinois at Urbana-Champaign Urbana, Illinois 61801	10. PROGRAM ELEMENT, PROJECT, TASK AREA & WORK UNIT NUMBERS 12, 11
11. CONTROLLING OFFICE NAME AND ADDRESS Joint Services Electronics Program	12. REPORT DATE (11) Jul[redacted]79
	13. NUMBER OF PAGES 72
14. MONITORING AGENCY NAME & ADDRESS (if different from Controlling Office)	15. SECURITY CLASS. (of this report) UNCLASSIFIED
	15a. DECLASSIFICATION/DOWNGRADING SCHEDULE

16. DISTRIBUTION STATEMENT (of this Report)

Approved for public release; distribution unlimited.

17. DISTRIBUTION STATEMENT (of the abstract entered in Block 20, if different from Report)

18. SUPPLEMENTARY NOTES

19. KEY WORDS (Continue on reverse side if necessary and identify by block number)

Surface Acoustic Waves
Line Acoustic Waves
Transducers and Reflectors

20. ABSTRACT (Continue on reverse side if necessary and identify by block number)

A non-iterative variational technique for solving the acoustic field equations is applied to three different boundary conditions, namely, a free surface, an edge and a surface with periodic discontinuities. A perturbation approach to surface wave scattering by periodic discontinuities is also developed and used to obtain both the elastic and the piezoelectric scatter matrix of a single electrode in a periodic array directly from the material parameters of the substrate and the electrodes. This scatter matrix accurately predicts the response of surface wave filters, transducers and reflectors.

DD FORM 1 JAN 73 1473 EDITION OF 1 NOV 65 IS OBSOLETE

UNCLASSIFIED 0977

SECURITY CLASSIFICATION OF THIS PAGE (When Data Entered)

UILU-ENG 78-2242

THEORY OF GUIDED ACOUSTIC WAVES IN PIEZOELECTRIC SOLIDS

by

Supriyo Datta

This work was supported in part by the Joint Services Electronics Program (U.S. Army, U.S. NAVY, AND U.S. Air Force) under Contract DAAG-29-78-C-0016 and N00014-79-C-0424; and in part by the U. S. Air Force under Contract F19628-78-C-0040.

THEORY OF GUIDED ACOUSTIC WAVES IN PIEZOELECTRIC SOLIDS

BY

SUPRIYO DATTA

B.Tech., Indian Institute of Technology, 1975
M.S., University of Illinois, 1977

THESIS

Submitted in partial fulfillment of the requirements
for the degree of Doctor of Philosophy in Electrical Engineering
in the Graduate College of the
University of Illinois at Urbana-Champaign, 1979

Thesis Advisor: Professor Bill J. Hunsinger

Urbana, Illinois

THEORY OF GUIDED ACOUSTIC WAVES IN PIEZOELECTRIC SOLIDS

Supriyo Datta, Ph.D.
Coordinated Science Laboratory and
Department of Electrical Engineering
University of Illinois at Urbana-Champaign, 1979

A non-iterative variational technique for solving the acoustic field equations is applied to three different boundary conditions, namely, a free surface, an edge and a surface with periodic discontinuities. A perturbation approach to surface wave scattering by periodic discontinuities is also developed and used to obtain both the elastic and the piezoelectric scatter matrix of a single electrode in a periodic array directly from the material parameters of the substrate and the electrodes. This scatter matrix accurately predicts the response of surface wave filters, transducers and reflectors.

Acknowledgements

I would like to thank my advisor Prof. Bill Hunsinger and my colleagues, particularly Mike Hoskins, Don Malocha and Steve Wilkus, for their help and understanding. The experimental work quoted in Chapter 3 would not be possible without Mike.

I thank Laura Ruggieri for her patient and skillful typing of the manuscript. I would also like to thank Susan Marshall for her help.

Table of Contents

List of Illustrations

Chapter 1: Introduction

Over the past decade a new technology has emerged using surface acoustic waves (SAW) for signal processing applications in the upper VHF and UHF range. These applications include miniature bandpass filters, resonators, convolvers, correlators and Fourier transformers [1]. The chief advantage of acoustic waves over their electromagnetic counterparts arises from the fact that acoustic velocities in solids are typically $\sim 10^{-5}$ times the velocity of light; the acoustic wavelength at 100 MHz is about 30μm compared to the electromagnetic wavelength of 3 meters. A significant miniaturization of signal processing components is thus achieved. Surface waves have proved particularly useful in this context because their energy is confined within a wavelength of the surface and is accessible all along the propagation path. Moreover, unlike most guided waves, surface waves are non-dispersive.

Most signal processing devices employ surface waves in piezoelectric anisotropic solids. Periodic arrays of electrodes are fabricated on the surface to interact with the wave and produce the desired results. An accurate description of these interactions is essential to proper filter design. The main objective of this thesis is to develop, from basic field theory, simple models describing these interactions that can be used by the device designer.

The following chapters deal with a variety of interesting acoustic field problems. Most of these results have already been published and the purpose of this thesis is to provide a compact outline of the approaches used. Detailed discussions of the techniques and references to the literature are available in the publications. A short tabulation of the contents of each

chapter and the relevant publications are listed below:

Chapter No.	Description	Reference
2	A method for obtaining the velocity and field distributions of surface waves along the free surface of a single or laminated anisotropic, piezoelectric medium.	2
3	A theoretical and experimental study of non-dispersive waves along an edge.	3,4,5,6
4	A method for calculating the approximate dispersion curves for surface waves in a medium with periodic surface perturbations.	7,8
5	A simple theory based on the concept of power exchange for describing the evolution of a propagating wave in the presence of source distributions.	9
6	Derivation of the piezoelectric scattering matrix for surface waves from an electrode in a periodic array.	10
7	Derivation of the mechanical scattering matrix for surface waves from an electrode in a periodic array.	11,12
8	A scatter matrix formulation for multistrip couplers used to couple surface waves from one track to another.	13
9	Transducer structures for optimum coupling to surface and line waves.	14
10	Application of the principle of superposition for simplified transducer design.	15,16,17,18

Chapters 2, 3 and 4 describe a non-iterative variational technique for solving the acoustic field equations as applied to three different boundary conditions. The same basic technique is applied in Chapter 2 to describe waves confined near a surface and in Chapter 3 to describe waves confined near an edge. Chapter 4 describes surface waves in a medium with periodic discontinuities at the surface. This technique has been used to

calculate the dispersion curves for surface waves in a periodic array of electrodes. However, it is sometimes difficult to get a converged solution using a reasonable number of terms in the expansion of the field quantities. An alternative perturbation approach to the problem is described in the remainder of the thesis.

Chapter 5 describes a simple perturbation theory that is used in the later chapters to characterize the interaction of surface waves with a periodic electrode array. This theory describes the generation of surface acoustic waves by sources such as charge and stress distributions. The scattering problem is then treated as a process of generation by sources induced by the interaction of an unperturbed wave with the discontinuity.

The effect of an electrode in a periodic array on a propagating acoustic wave is described conveniently in terms of a scatter matrix that relates the outgoing acoustic waves and the current into the electrode to the incoming acoustic waves and the electrode voltage (Fig. 6.2, Eq. 6.7). Chapters 6 and 7 evaluate the piezoelectric and the mechanical parts of the first two columns (Eq. 6.7) of the scatter matrix respectively, while Chapters 9 and 10 involve the last column of the scatter matrix. Chapter 8 describes a scatter matrix formulation for multistrip couplers which are widely used in surface wave devices as beam compressors and track changers. The scatter matrix elements are deduced from the results of Chapter 6.

Chapter 2: Surface Acoustic Waves

Surface acoustic waves are non-dispersive waves along the surface of a solid and decay exponentially in the direction normal to the surface (Fig. 2.1). The velocity and field distributions for surface waves are usually obtained using an iterative procedure to satisfy the boundary conditions at the interface [19]. This procedure is rather complicated especially in layered structures [20] where boundary conditions have to be satisfied at several interfaces.

This chapter describes a non-iterative technique for obtaining surface wave solutions in anisotropic piezoelectric solids [2]. The boundary conditions are incorporated into the acoustic field equations using position-dependent material constants. This makes it possible to account for the boundary conditions directly without iteration even in laminated media with several interfaces. To find the velocity and field distributions typically requires the diagonalization of a 30x30 matrix which takes only a few seconds on a computer.

The coordinate axes x_1, x_2, x_3 are chosen so that the wave propagates in the x_1-direction, decays in the x_2-direction and is uniform in the x_3-direction. The acoustic field is described by the particle displacements in the three directions u_1, u_2 and u_3. In piezoelectric solids there is an accompanying electrostatic field described by the electrostatic potential, ϕ. The stress, T and the electrical displacement, D are related to the field quantities u and ϕ by the constitutive relations:

$$T_{ac} = C_{acbd} \frac{\partial u_b}{\partial x_d} + e_{dac} \frac{\partial \phi}{\partial x_d} \qquad (2.1a)$$

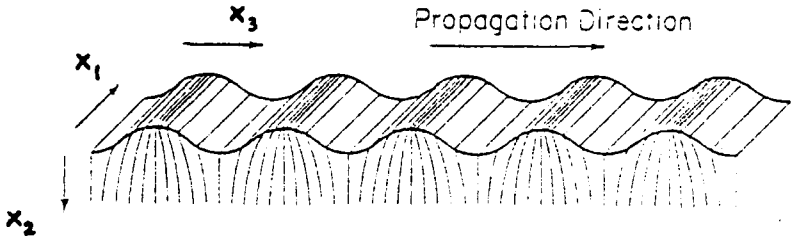

Figure 2.1: Surface waves in a semi-infinite medium

$$D_c = e_{cbd} \frac{\partial u_b}{\partial x_d} - \epsilon_{cd} \frac{\partial \phi}{\partial x_d} \tag{2.1b}$$

where C, e and ϵ are the stiffness, piezoelectric and permittivity tensors of the medium. The indices a, b, c, d take on the values 1, 2, 3 and summation over repeated subscripts is implied. The field equations are:

$$\frac{\partial T_{ac}}{\partial x_c} = -\rho\omega^2 u_a \tag{2.2a}$$

$$\frac{\partial D_c}{\partial x_c} = 0 \tag{2.2b}$$

where ρ is the mass-density of the solid. The first equation is obtained by equating the force on a differential element to its mass times its acceleration and assuming an exp(jωt) dependence for all field quantities. The second equation is Laplace's equation from electrostatics.

Using the constitutive relations (2.1) to substitute for T and D in the field equations (2.2) we obtain differential equations relating the field quantities u and ϕ. For a homogeneous medium the material constants C, e and ϵ are constants so that the differential equations have constant coefficients. In a laminated medium, the usual procedure is to solve these equations separately for each of the layers and then look for the correct wavenumber at which the normal stresses and electrical displacement are continuous at the interfaces. For a semi-infinite solid this involves making the normal stresses zero at the surface.

In the present approach the material constants are written as functions of x_2 so as to describe the composite medium. For a semi-infinite solid we write,

$$\bar{F}(x_2) = F \cdot \theta(x_2) \tag{2.3a}$$

where F denotes any of the material constants ρ, C, e or ϵ of the substrate. $\bar{F}$ is its position-dependent value, $\theta(x_2)$ being the unit step function. For a layered medium we write,

$$\bar{F}(x_2) = F\ \theta(x_2-h) + F'[\theta(x_2) - \theta(x_2-h)] \tag{2.3b}$$

where F is the material constant of the substrate while F' is that of the layer on top, of thickness h.

Using this method, we have a single differential equation with variable coefficients for the composite medium. The field equations involve derivatives of the material constants giving rise to delta functions at the interfaces that take care of the boundary conditions automatically [21].

To solve this composite differential equation, the field quantities u_a and ϕ are expanded in a series of orthogonal functions. We know that the excitations are wavelike along x_1 and decay essentially exponentially along x_2. In view of this, the field quantities are expanded in a series of Laguerre functions in x_2. The Laguerre functions form a complete orthonormal set over $(0,\infty)$ and are defined as,

$$|m(q)\rangle = \exp(-\tfrac{q}{2}).\ P_m(q)/m! \tag{2.4}$$

where P_m is the m^{th} Laguerre polynomial. The presence of the exponential term is particularly convenient for the decaying field distributions we are seeking to describe. It is found that five terms in the expansion provide an adequate description of the field. In the propagation direction the fields are assumed wavelike with a $\exp(-jkx_1)$ dependence, k being the wavenumber.

Using this expansion the differential equation is converted to an algebraic matrix equation. The matrix elements are determined from integrals involving the position-dependent material constants. The unknowns are the expansion coefficients of the various field quantities. The lowest eigenvalue of the matrix yields the velocity of the surface wave and the corresponding eigenvector gives the field distributions.

This technique has been applied to obtain surface wave solutions for various orientations of lithium niobate ($LiNbO_3$); dispersion curves have been computed for practical layered structures such as silicon dioxide on lithium tantalate and gold on $LiNbO_3$. Fig. 2.2 shows the surface wave velocity against kh where k is the wavenumber and h is the thickness of the gold layer. This is in agreement with results reported earlier using iterative techniques [22]. The details have been described in refs. [2] and [7].

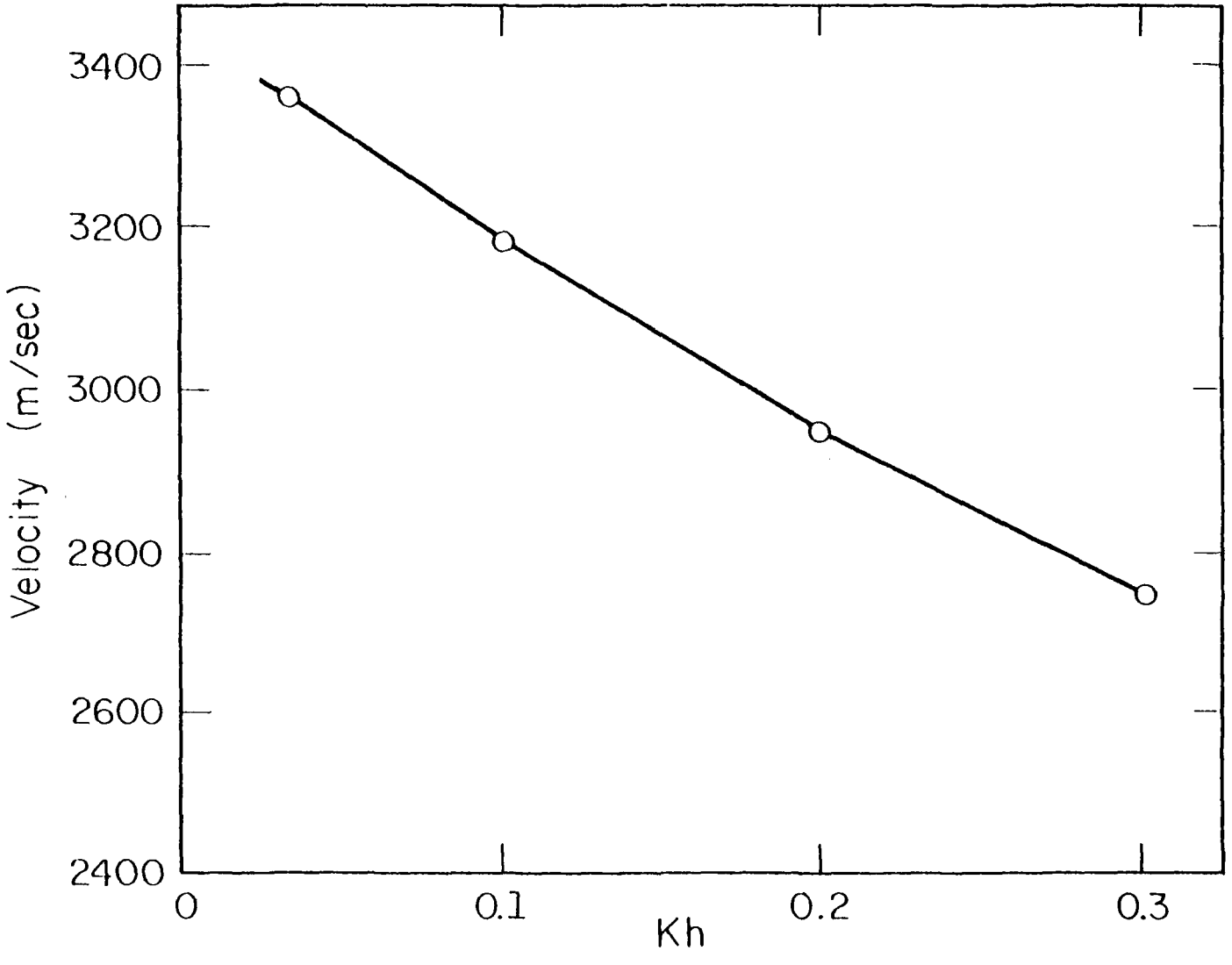

Figure 2.2: Surface wave velocity in a laminated medium with gold of thickness h on a semi-infinite $LiNbO_3$ substrate

KP-1572

Chapter 3: Line Acoustic Waves

The guiding of surface acoustic waves along a free surface involves only one boundary in contrast to most waveguiding structures which require two boundaries. This makes surface waves non-dispersive since the guiding structure has no characteristic dimension.

The guiding action of the surface is explained qualitatively in this way. The particles near the surface have greater freedom of movement than those within the bulk of the solid. This makes the surface appear less "stiff" than the bulk so that the wavefront moves slower near the surface. Since waves in general tend to be guided along regions of lower velocity the surface acts as a guide.

This view of surface guiding leads us to expect that there will be a further lowering of wave velocity near an edge formed by two stress-free surfaces. These waves, called line acoustic waves, are non-dispersive too since an edge has no characteristic dimensions. In addition line acoustic waves are diffractionless and the total energy remains confined within a square wavelength from the edge.

The theoretical analysis of surface waves described in chapter 2 is readily extended to line waves by using a double series of Laguerre functions to expand the decaying field distributions along both x_2 and x_3 [3]. Using this analysis the field distribution for a z-propagating line wave in lithium niobate was calculated. A computer plot is shown in Fig. 3.1. It is seen that the wave motion is flexural. The particle motion is antisymmetric about a central plane; when the horizontal face moves into the solid, the vertical face moves out of the solid thus making room for each other. As may be expected, this is the mode with the

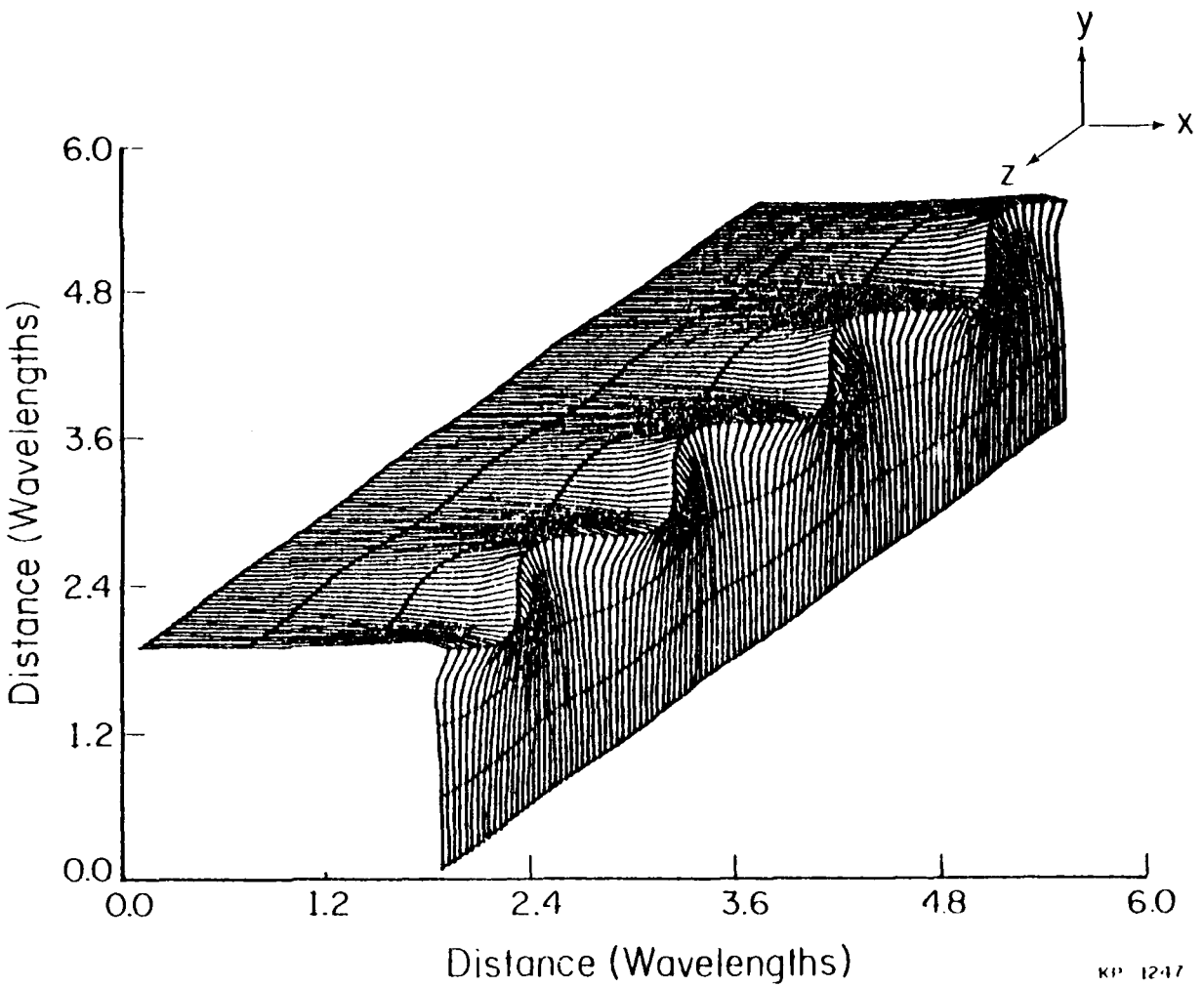

Figure 3.1: Computer plot of line acoustic waves in Y-cut $LiNbO_3$

lowest velocity; symmetric modes where the two faces move in and out in synchronism have higher velocities and in most cases are not guided modes.

Line waves are characterized by high power density, zero diffraction and nondispersive propagation which make them suitable for signal processing applications. However, for practical device applications we need edges that do not have imperfections any larger than a fraction of a wavelength; in the UHF range this means that chips and striations at the edge should be smaller than a micron.

We were able to obtain edges suitable for lossless non-dispersive propagation of line waves up to at least 220 MHz ($\lambda \approx 16\mu m$) by cleaving commercial lithium niobate crystals with top polished surfaces [4]. The cleavage plane in $LiNbO_3$ (012) lies along the x-axis at an angle of 57.24° to the y-axis [23]. Using different cuts of $LiNbO_3$ as the starting material, wedges with different interior angles are obtained as shown in Fig. 3.2.

For our experiments we used a wedge with an interior angle of 84.9° obtained by cleaving 127.86° rotated Y-cut $LiNbO_3$ (Fig. 3.3). Since the cleavage plane is crystallographically determined, the angle of the wedge is known very accurately. The theoretically calculated particle displacements and electrical potentials along the top surface are shown in Fig. 3.4 for a 100 mW line wave along this wedge.

Line waves at 40 MHz were excited using an interdigital transducer with 45 electrode pairs and a uniform overlap of 1λ. The shear particle displacement was measured along the top surface of the wedge using a laser probe [24]. The experimentally measured values show good agreement with the theoretical particle displacement profile (Fig. 3.5).

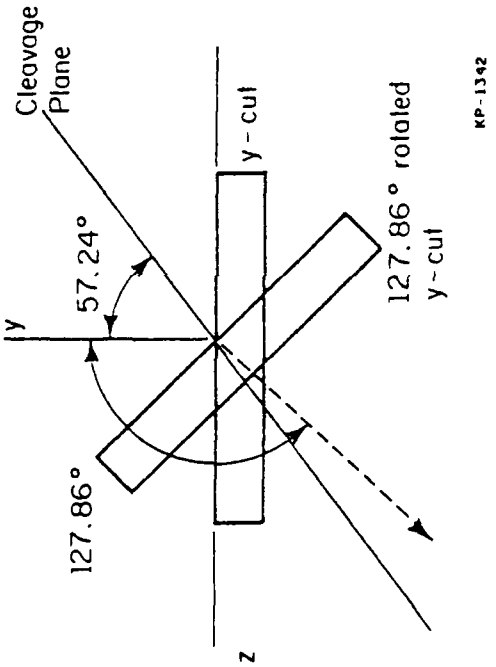

Figure 3.2: Fabrication of wedges with different corner angles by cleaving different cuts of $LiNbO_3$

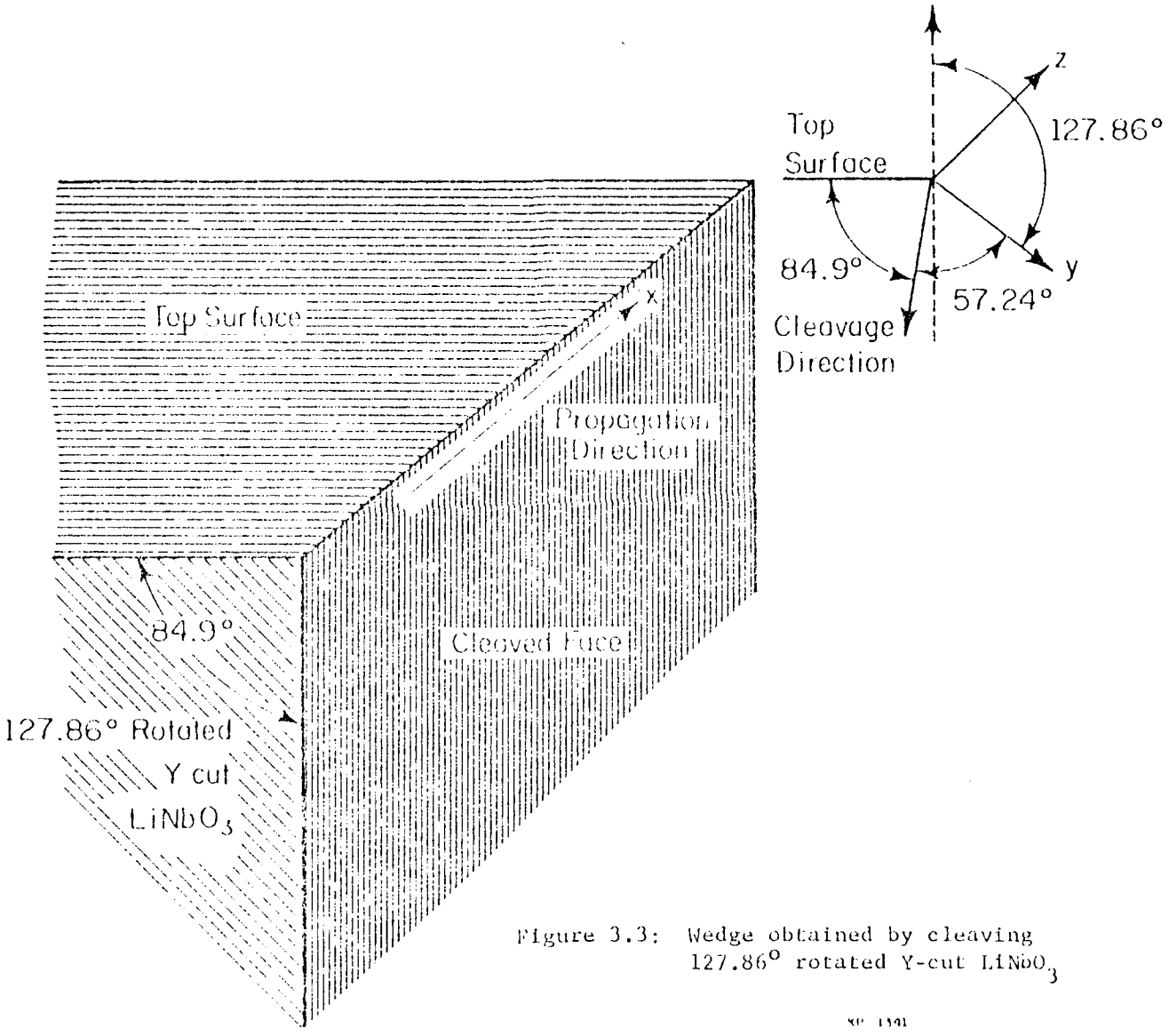

Figure 3.3: Wedge obtained by cleaving 127.86° rotated Y-cut $LiNbO_3$

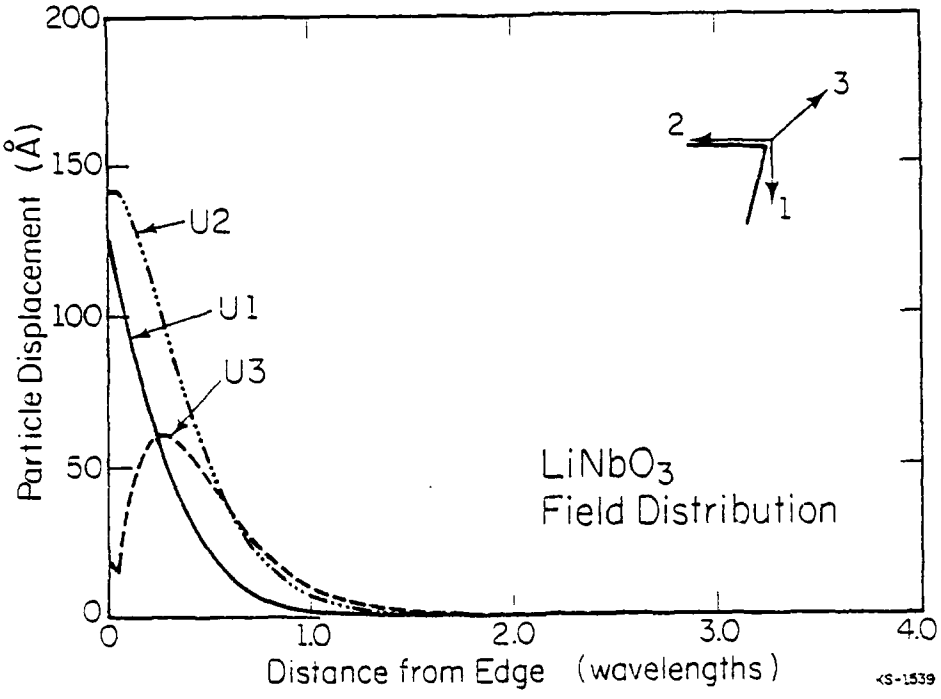

(a)

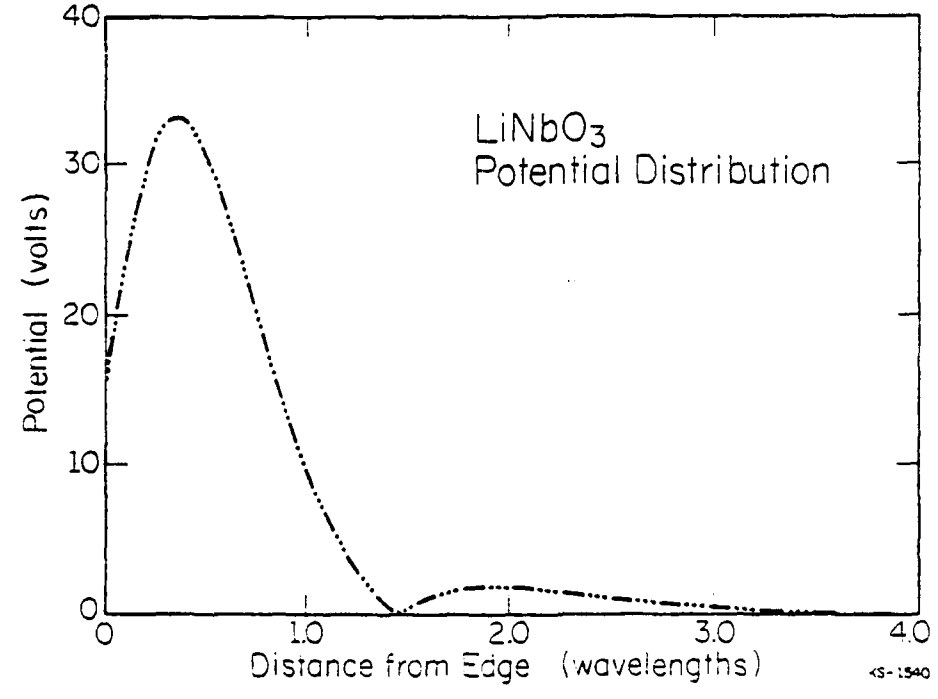

(b)

Figure 3.4: Fields along top wedge surface for a line wave carrying 100 mW
(a) Particle displacements
(b) Electrical potential

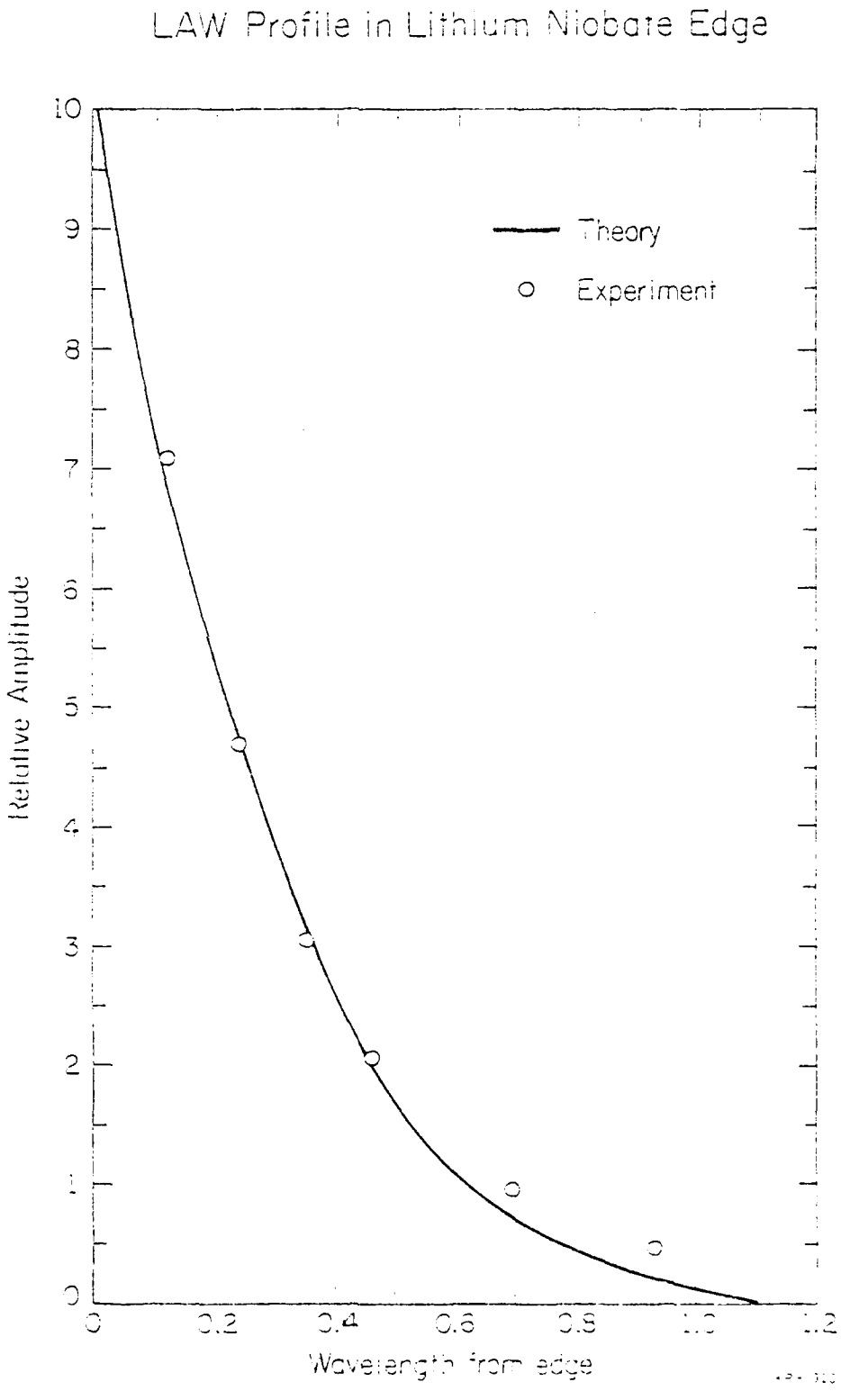

Figure 3.5: Particle displacement (shear) profile along top surface

The measured line wave velocity was 3500 m/sec. ($\pm$ 1%), which compares well with the theoretical value of 3488 m/sec.

A 220 MHz line wave device [5] was built using single phase transducers (Fig. 3.6). These transducers have electrodes $\lambda/2$ wide as compared to the $\lambda/8$ wide electrodes required for reflection-free interdigital transducers. This reduces the resolution requirements by a factor of 4 so that higher frequency devices are fabricated with the same photolithographic capability. Fig. 3.7 shows the frequency response of the device which has the ideal $(\text{Sin}x/x)^2$ shape anticipated for a non-dispersive delay line with unweighted transducers. No significant losses could be detected along a 1 cm. propagation path.

One of the drawbacks of the single phase transducer is its poorer coupling compared to the interdigital transducer. A sawtooth transducer (Fig. 3.8) combining some of the features of the interdigital and the single phase transducer, provides better coupling [6]. A discussion of the coupling efficiency of various types of transducers is contained in chapter 9.

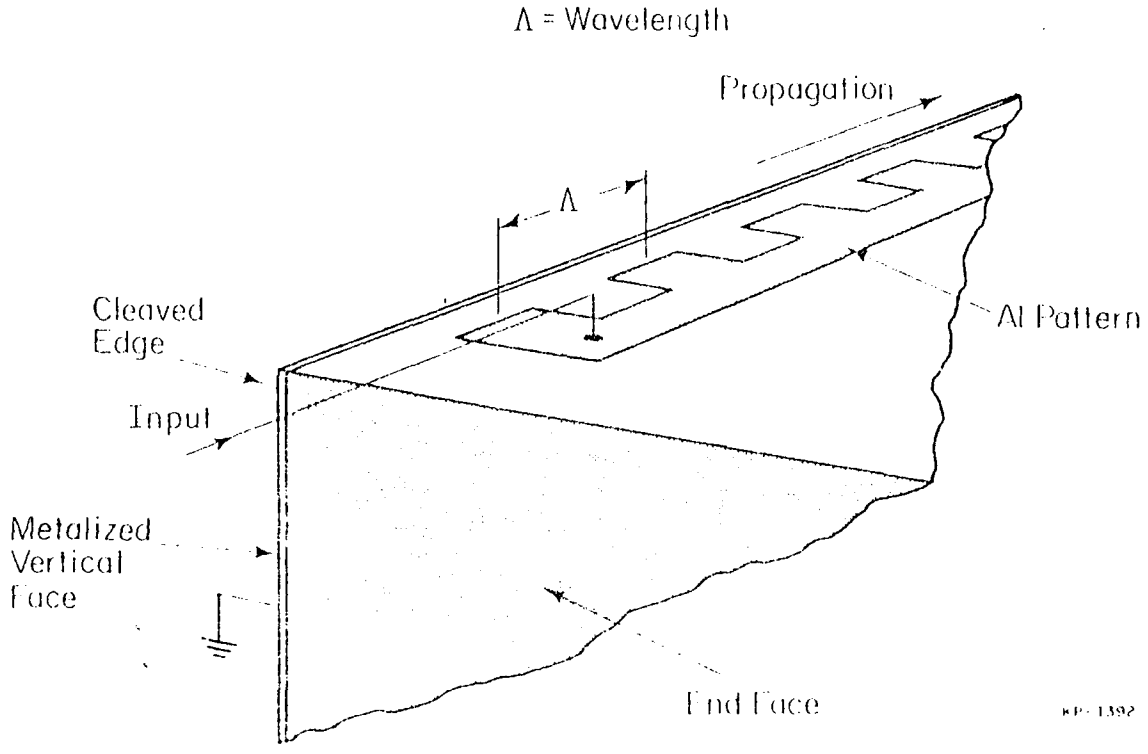

Figure 3.6: Single-phase transducer

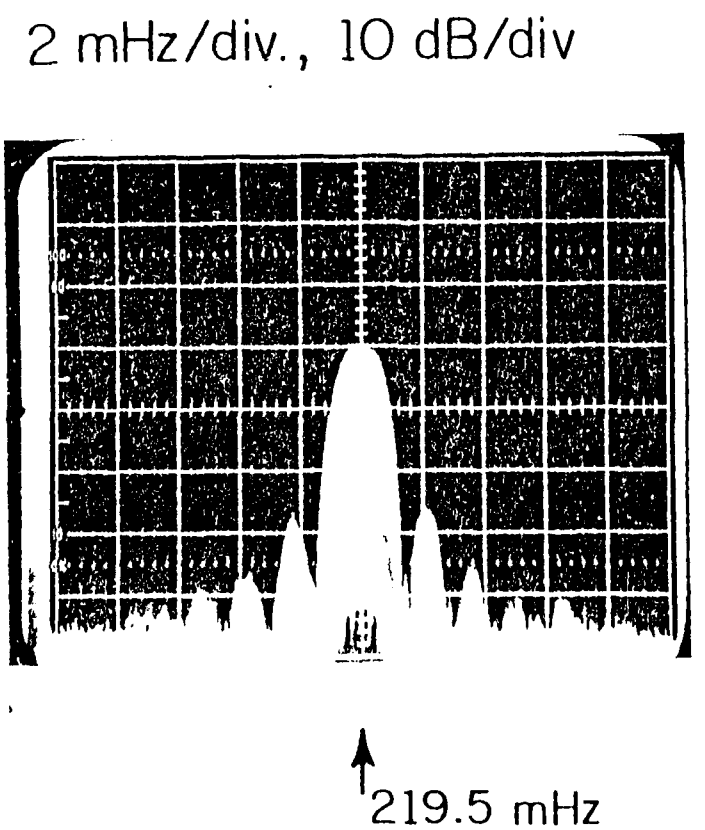

Figure 3.7: Measured frequency response of line acoustic wave delay line

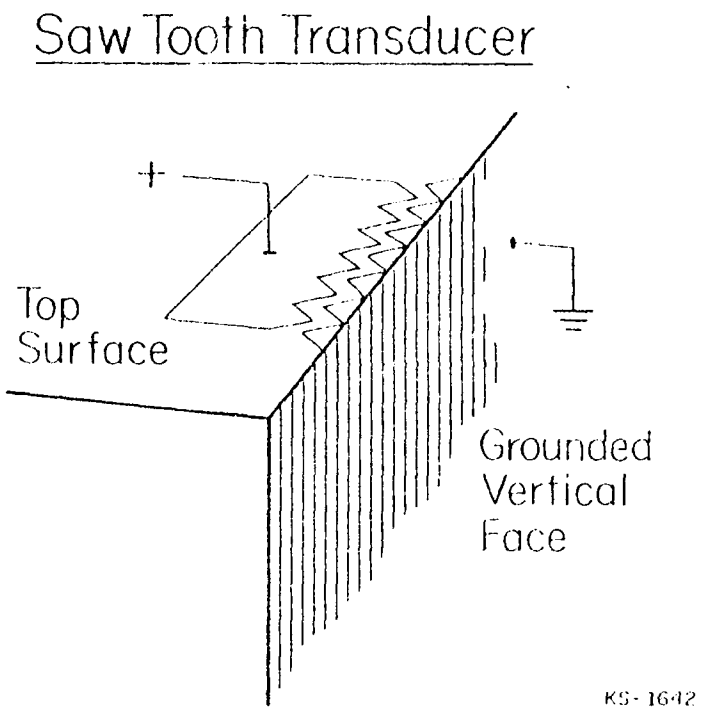

Figure 3.8: Sawtooth transducer

Chapter 4: SAW in Periodic Laminated Media

In chapter 2 an analysis of surface waves in laminated media was described using an orthonormal series of Laguerre functions to express field distributions in the direction perpendicular to the surface. However, the medium was assumed uniform in the propagation direction x_1, so that the field quantities were wavelike in x_1 with a single Fourier component $\exp(-jkx_1)$. We have extended this technique to include periodic variations of the material constants in the propagation direction (Fig. 4.1) by using Fourier series to express field distributions as required by Floquet's theorem:

$$f(x_1,x_2) = \sum_{m,n} f_{mn}\ \phi_m(x_2)\ \exp\left[-j\left(k+n\ .\ \frac{2\pi}{p}\right)\ x_1\right] \qquad (4.1)$$

where $\phi_m(x_2)$ is the Laguerre function

p = length of one period

and f_{mn} are the expansion coefficients for the field quantity f.

As before, using position-dependent material constants to describe the composite media we can take care of the complex boundary conditions in this problem. The differential equations are then converted to matrix equations and the phase velocity for a given wavenumber is obtained from the lowest matrix eigenvalue [7].

The chief difficulty of this method lies in the fact that many practical problems require a large number of Fourier terms for an accurate description of the fields. This makes the size of the final matrix unwieldy for the numerical computation of eigenvalues. Perhaps a different basis set for expressing field distributions in the propagation direction would be more appropriate. However, this has not been investigated.

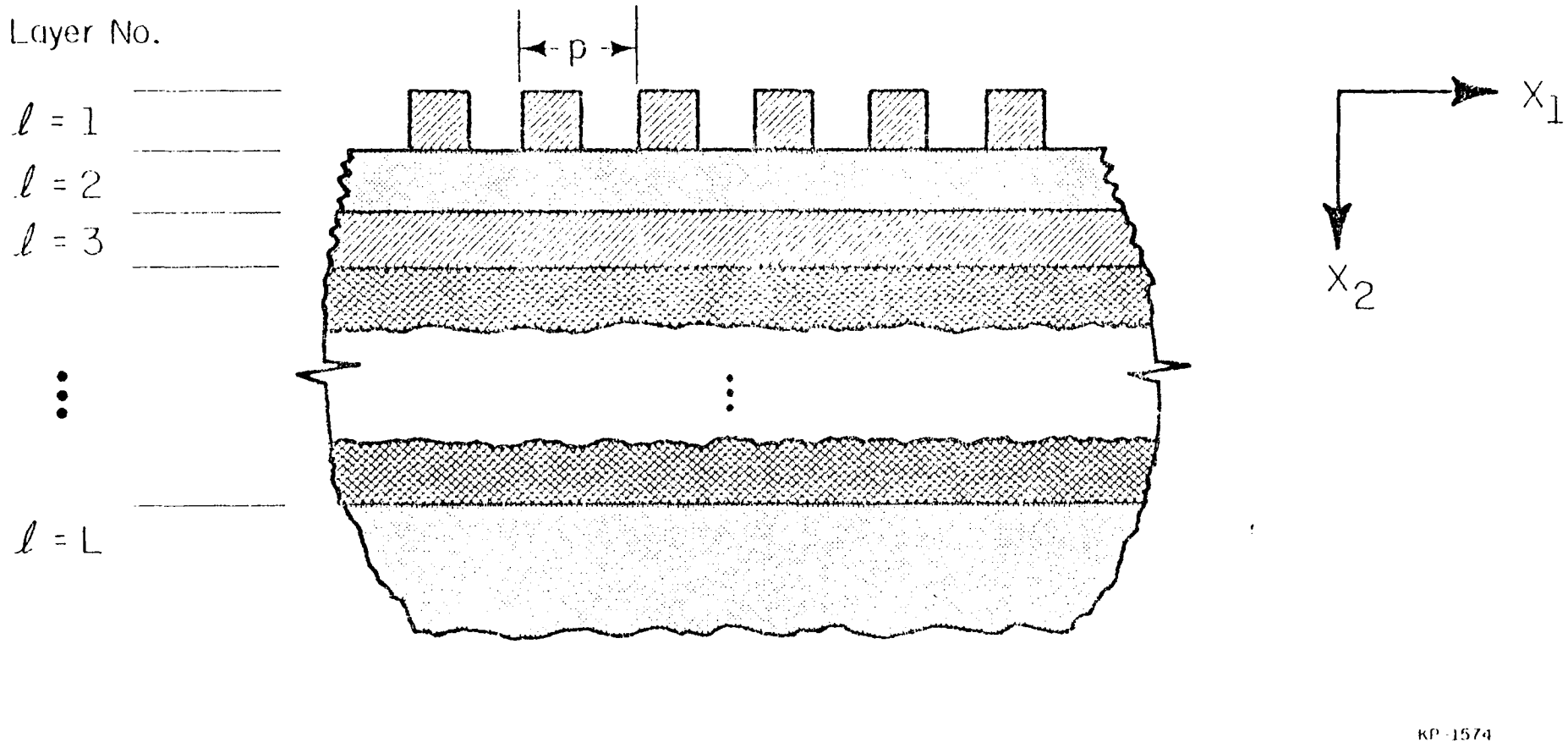

Figure 4.1: Laminated medium with periodic discontinuities

The technique was applied to various practical structures with considerable success. Fig. 4.2 shows the velocity for different wavenumbers, k, obtained for a grating of thin electrodes on Y-Z $LiNbO_3$. The wavenumber is normalized to $\beta_o (= 2\pi/p)$ where p is the grating period. At $k = .5\beta_o$ there is a stopband as anticipated. The velocity is discontinous at this point. The potential and charge distributions along the surface are shown in Fig. 4.3 corresponding to the two values of velocity. The flat potential regions correspond to the regions covered by electrodes. Between the electrodes the charge is expected to be zero. As can be seen from the figures, this boundary condition is only approximately satisfied. This is because only a finite number of Fourier terms is used. The present analysis is thus a variational analysis that minimizes the velocity eigenvalue for an assumed expansion of field quantities in orthogonal functions.

The method has also been applied to grooved arrays and thick electrodes. These results are described in [8]. This technique provides a generally applicable scheme for calculating approximate dispersion relations for laminated piezoelectric structures with periodic boundaries.

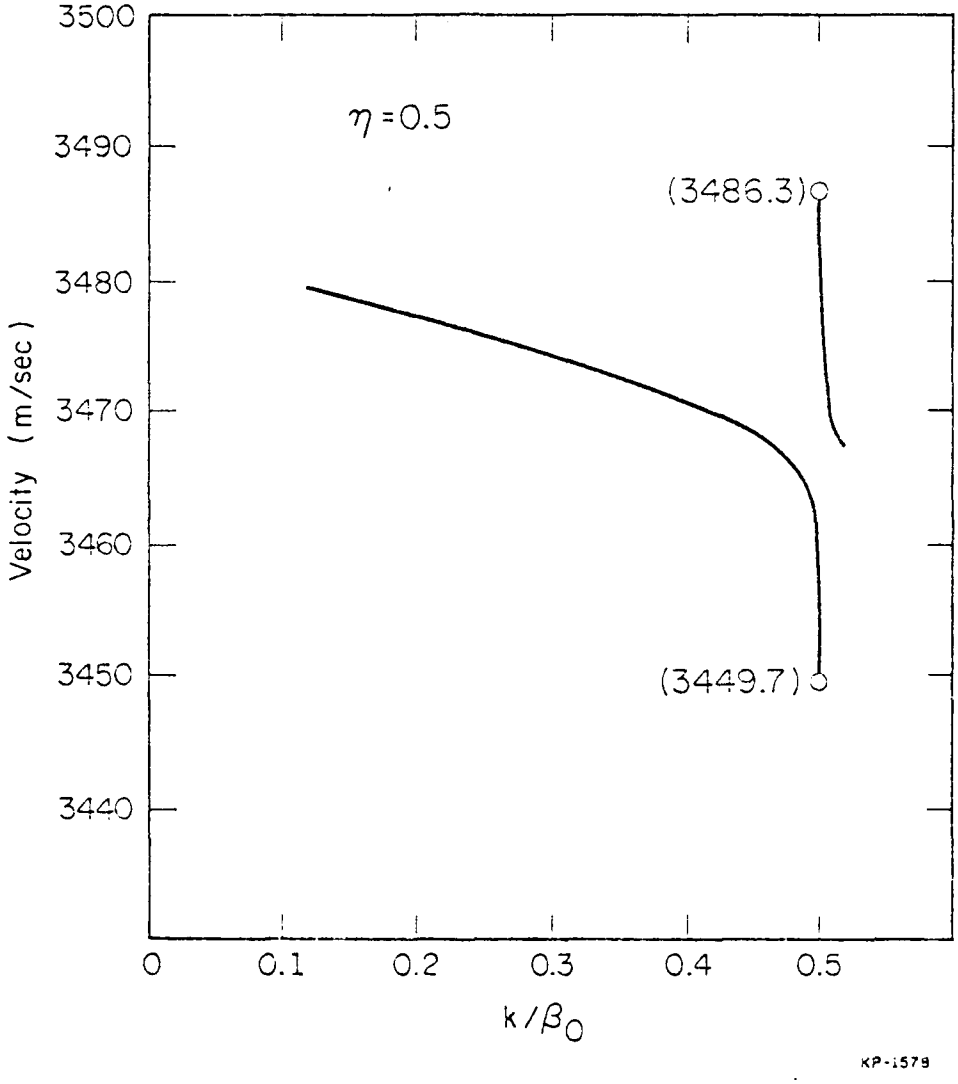

Figure 4.2: Dispersion curve for thin conductive grating on Y-Z $LiNbO_3$

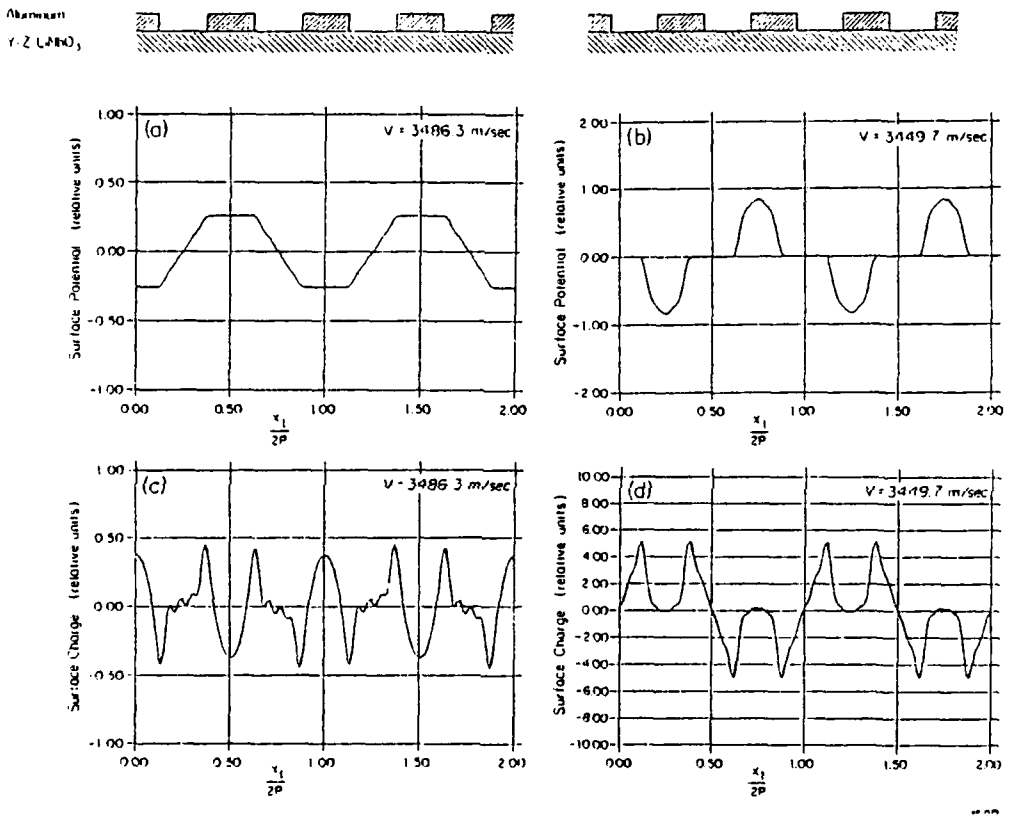

Figure 4.3: Thin conductive grating on Y-Z $LiNbO_3$

(a) Surface potential for higher velocity solution at k = .5 β_o

(b) Surface potential for lower velocity solution at k = .5 β_o

(c) Surface charge for higher velocity solution at k = .5 β_o

(d) Surface charge for lower velocity solution at k = .5 β_o

Chapter 5: A Simple Perturbation Theory for Propagating Waves

A commonly occurring problem in wave theory is to describe the changing characteristics of a propagating wave due to a distribution of sources in the medium. This source distribution may be due to external generators, as in transducers; or it may be induced by the incident wave due to a change in the material properties, as in reflectors. In most practical cases the perturbation of the wave is small over a wavelength, and no essential change takes place in the relationship between the different field components comprising the mode. Under these conditions even a complicated coupled mode like a Rayleigh wave is described by a single complex amplitude, A. An unperturbed wave travelling in the z-direction has a constant amplitude A; in the presence of sources the wave is perturbed and A is a slowly varying function of z described by a simple differential equation (Fig. 5.1):

$$\frac{1}{A}\frac{dA}{dz} = \frac{1}{2P_a}\frac{dP}{dz} \tag{5.1}$$

where (1) dP is the power (active and/or reactive) flowing from the source into the wave in a distance dz along the propagation path.

and (2) P_a is the time-averaged power flow of the propagating wave.

This equation follows quite easily for real dP from the relation $P_a \sim |A|^2$ and the conservation of power. For imaginary (or reactive) dP the relation is not so obvious but can be proved by considering the instantaneous (rather than time-averaged) power flow.

Equation (5.1) is simple in appearance but is remarkably versatile in solving the type of perturbation problems we have been discussing. Its applicability ranges from the simple case of a plane wave in a transmission line to the more complicated case of guided acoustic waves in piezoelectric

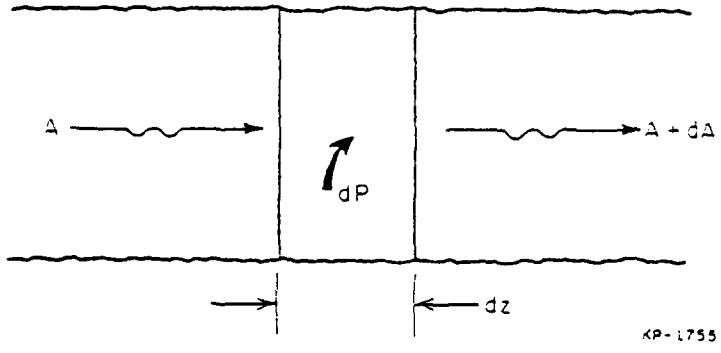

Figure 5.1: Mode amplitude change in the presence of driving sources

media, as we propose to show with the following examples. The results presented here are not new, but they are all derived from the same equation (5.1), thus providing a simple unified physical picture for a wide variety of wave perturbation phenomena. This makes it straightforward to extend the results to new problems involving waves with more complicated fields.

1. A classical transmission line:

We start with a trivial example for which exact solutions are available from well-known conventional techniques and show how Eq. (5.1) predicts the same results. We consider a transmission line modeled as a distributed circuit with a series impedance, Z and a shunt admittance, Y. The characteristic impedance, Z_o and the propagation constant, γ_o are related to Z and Y by,

$$Z_o = \sqrt{\frac{Z}{Y}} \tag{5.2a}$$

$$\gamma_o = \sqrt{ZY} \tag{5.2b}$$

Now if we change the shunt admittance by an amount ΔY, the propagation constant will change from γ_o to $\gamma_o + \Delta\gamma$.

$$\gamma_o + \Delta\gamma = \sqrt{Z(Y + \Delta Y)}$$

$$\simeq \gamma_o \left(1 + \frac{\Delta Y}{2Y}\right) \text{ if } \Delta Y \ll Y$$

so that,

$$\Delta\gamma = \frac{\gamma_o}{2} \cdot \frac{\Delta Y}{Y} \tag{5.3}$$

provided ΔY is much less than Y; that is, if the perturbation is small.

Now we derive $\Delta\gamma$ using Eq. (5.1). The additional admittance ΔY causes a shunt current, I_s per unit length given by

$$I_s = V \cdot \Delta Y$$

where V is the potential of an unperturbed wave. This shunt current I_s may be considered an induced "source" and the power flow into the wave from this source in a distance dz is written as,

$$dP = -\frac{1}{2} V^* I_s \, dz$$

$$= -\frac{|V|^2}{2} \Delta Y \, dz \qquad (5.4)$$

Using dP from (5.4) in (5.1),

$$\frac{1}{A}\frac{dA}{dz} = -\frac{|V|^2}{4P} \cdot \Delta Y$$

$$= -\frac{Z_o}{2} \cdot \Delta Y \qquad (5.5)$$

Integrating (5.5), we have,

$$A(z) = A_o \exp(-\Delta\gamma z) \qquad (5.6)$$

where, A_o is a constant

and, $$\Delta\gamma = \frac{Z_o}{2} \cdot \Delta Y \qquad (5.7)$$

The results in Eqs. (5.3) and (5.7) are seen to be equivalent, noting from Eq. (5.2) that $Z_o Y = \gamma_o$. The amplitude A used here can be any of the field quantities (voltage or current) with the unperturbed phase factor $\exp(-\gamma_o z)$ removed.

2. Plane bulk acoustic waves in a conducting medium:

We now go on to a more complicated example. Let us consider a plane bulk acoustic wave propagating in an insulating solid with a piezoelectrically stiffened velocity v_a. The wave is accompanied by a traveling electrical potential ϕ_a. We wish to find the attenuation and the change in velocity of this wave if the solid has a finite conductivity σ and a dc field

is impressed to drift the carriers in the propagation direction. Exact solutions for this situation are available [25] and once again we can compare our results from Eq. (5.1) with well-known results.

In a conducting medium the piezoelectric potential ϕ_a due to the acoustic wave causes the charges to bunch, forming a traveling wave charge distribution ρ. This charge distribution produces an electrostatic potential, ϕ_e that is obtained from Poisson's equation.

$$\rho = \beta_o^2 \epsilon \phi_e \tag{5.8}$$

where ϵ is the permittivity of the medium and β_o is the unperturbed wavenumber of the acoustic wave. For small perturbations we may ignore the difference between β_o and the perturbed wavenumber β and replace $\partial/\partial z$ by $-j\beta_o$. Since we are considering plane waves, we have set $\partial/\partial x = \partial/\partial y = 0$.

Let J be the current per unit area due to the traveling charge distribution. This current is considered the source from which the acoustic wave absorbs a power, dP, per unit area given by,

$$dP = -\frac{1}{2}\,\phi_a^*\left(\frac{\partial J}{\partial z}\right) \cdot dz \tag{5.9}$$

From current continuity,

$$\frac{\partial J}{\partial z} = -j\omega\rho \tag{5.10a}$$

or,

$$J = v_a \rho \tag{5.10b}$$

$v_a = \omega/\beta_o$ being the acoustic wave velocity. Using (5.10a) in (5.9), we have,

$$\frac{dP}{dz} = \frac{\phi_a^*\,(j\omega\rho)}{2} \tag{5.11}$$

so that, from Eq. (5.1),

$$\frac{1}{A}\frac{dA}{dz} = \frac{\phi_a^* (j\omega\rho)}{4P_a} \tag{5.12}$$

where P_a is the power flow per unit area of the acoustic wave. In this example the wave in the insulating solid was assumed the unperturbed mode. The acoustic wave thus has no associated charge ρ_a. However, in general we should add a term $(j\omega\rho_a)^* \phi_e$ to the numerator in (5.12).

We now need the charge distribution ρ in terms of ϕ_a to complete the analysis. This is readily done by writing J from the material constants and using Eq. (5.10b).

$$J = v_a\rho = j\beta_o\sigma(\phi_a + \phi_e) + v_d\rho + j\beta_o D\rho \tag{5.13}$$

where, (1) σ is the conductivity of the medium

(2) D is the diffusion constant of the carriers

(3) v_d is the drift velocity of the carriers in the propagation direction due to an external dc field.

Here we have written only the linear component of current having $\exp(-j\beta_o z)$ dependence. The non-linear acoustoelectric component involving the product of ϕ and ρ is neglected. Using Eq. (5.8), we obtain from (5.13),

$$j\omega\rho = \frac{-\beta_o^2 \sigma\phi_a}{\gamma - j\left(\frac{\omega_c}{\omega} + \frac{\omega}{\omega_d}\right)} \tag{5.14}$$

where, $\gamma = 1 - v_d/v_a$ (drift parameter) (5.15a)

$\omega_c = \sigma/\epsilon$ (conductivity relaxation frequency) (5.15b)

$\omega_d = v_a^2/D$ (diffusion frequency) (5.15c)

Using (5.14) in (5.12),

$$\frac{1}{A}\frac{dA}{dz} = -\frac{\phi_a \phi_a^*}{4P_a} \frac{\beta_o^2\sigma}{\gamma - j\left(\frac{\omega_c}{\omega} + \frac{\omega}{\omega_d}\right)}$$

so that, $A = A_o \exp[-(\alpha + j\Delta\beta)z]$

where

$$\frac{\alpha}{\beta_o} + j\frac{\Delta\beta}{\beta_o} = \frac{\phi_a \phi_a^*}{4P_a} \frac{\beta_o \sigma}{\gamma - j\left(\frac{\omega_c}{\omega} + \frac{\omega}{\omega_d}\right)} \tag{5.16}$$

Here α is the attenuation constant and $\Delta\beta$ is the change in the wavenumber. Now, for a perfectly conducting medium with no drift field, we can obtain the change in wavenumber $\Delta\beta_{sc}$ from (5.16):

$$\frac{\Delta\beta_{sc}}{\beta_o} = \frac{\phi_a \phi_a^*}{4P_a} \cdot \beta_o \omega \epsilon \tag{5.17}$$

Using (5.17) in (5.16),

$$\frac{\alpha}{\beta_o} + j\frac{\Delta\beta}{\beta_o} = \frac{\Delta\beta_{sc}}{\beta_o} \frac{\omega_c/\gamma\omega}{1 - \frac{j\omega_c}{\gamma\omega}\left(1 + \frac{\omega^2}{\omega_c \omega_d}\right)} \tag{5.18}$$

This is seen to be the same result as in [25] noting that $\Delta\beta_{sc}/\beta_o$ is equal to half the electromechanical coupling constant.

3. Surface acoustic waves in the presence of distributed sources:

Now we come to an example for which no exact solutions are available, namely the propagation of a surface wave in the presence of stress and charge distributions on the surface and distributed volume forces and charges within the bulk.

Consider an unperturbed surface wave propagating with a velocity c_s along the surface of a semi-infinite substrate with a perfect open circuit ($\epsilon = 0$) above. The propagation is in the z-direction and the wave is assumed uniform in the x-direction. Now if we assume stress distributions $T'_{iy}(z)$ (i = x,y,z) and an electrical displacement $D'_y(z)$ on the surface (y = 0) then the power dP_s flowing into the surface wave per unit beam

width in a distance dz is given by,

$$dP_s = A^* \cdot \frac{1}{2}\, dz \left[-\sum_{i=x,y,z} v_i^*(y=0)\; T'_{iy} + \phi^*(y=0)\; j\omega D'_y \right] \qquad (5.19)$$

where A is the amplitude of the surface wave and $v_i(y=0)$, $\phi(y=0)$ represent the particle velocity and electrical potential at the surface of a unit amplitude unperturbed surface wave. The signs of the terms in (5.19) correspond to the y-direction being into the surface.

If there is a body force density F' and a charge density ρ' within the volume then there is an additional power flow dP_v into the surface wave given by,

$$dP_v = A^* \cdot \frac{1}{2}\, dz \int_0^\infty dy \left[\sum_{i=x,y,z} v_i^*\, F'_i + \phi^*(j\omega\rho') \right] \qquad (5.20)$$

The total power flow into the wave is,

$$dP = dP_s + dP_v \qquad (5.21)$$

Now, from Eq. (5.1) we have,

$$\frac{1}{A}\,\frac{dA}{dz} = \frac{1}{2|A|^2 P_n}\,\frac{dP}{dz} \qquad (5.22a)$$

where P_n is the power carried by a unit amplitude surface wave, so that the power in a surface wave of amplitude A is given by

$$P_a = |A|^2\, P_n. \qquad (5.22b)$$

Using (5.19), (5.20) and (5.21) in (5.22a),

$$4\, P_n\, \frac{dA}{dz} = f_s + f_v \qquad (5.23)$$

where,

$$f_s = -\sum_{i=x,y,z} v_i^*(y=0)\; T'_{iy} + \phi^*(y=0)\; j\omega D'_y \qquad (5.24a)$$

$$f_v = \int_0^\infty dy \left[\sum_{i=x,y,z} v_i^* F_i' + \phi^* (j\omega\rho') \right] \qquad (5.24b)$$

Here the primed quantites represent sources while unprimed quantites are the fields due to the unperturbed wave. As noted in connection with bulk waves, the unperturbed mode is assumed not to have any stresses T_{iy} or electrical displacement D_y at the surface; nor any forces F_i or charges ρ within the volume. Otherwise, the corresponding power flow terms (such as $\{j\omega D_y(y=0)\}^* \cdot \phi'$, ϕ' being the source potential) have to be added to f_s and f_v.

Eq. (5.23) is really the well-known normal-mode equation for surface waves that was derived from the reciprocity theorem [26]. It is the starting point for numerous problems involving surface wave transducers, reflectors and amplifiers. It is interesting to note that it follows from the trivial-looking relation (5.1). The appropriate equation for more complicated fields as in guided surface waves can also be written down by inspection.

To summarize, we have shown that the perturbation of any wave by impressed or induced sources is described by the simple relationship stated in Eq. (5.1). The application of this principle is illustrated with three examples--the classical transmission line, the propagation of plane acoustic waves in conductive media and the generation of SAW by impressed stresses and charges. We believe that this provides a simple unified picture of wave perturbation that will prove useful in the treatment of newer and more complicated problems.

Chapter 6: Piezoelectric Scatter Matrix for Thin Conductive Gratings

Periodic arrays of thin metallic electrodes are widely used in surface wave devices for constructing transducers and reflectors. In reflectors the electrodes are either left unconnected or shorted together to form a periodic grating so that the structure is truly periodic. In transducers, however, the electrodes are connected to external voltage sources and the particular sequence and phasing of electrode voltages depends on the desired spectral response [27]. This makes the structure electrically non-periodic. The analysis to be described in this chapter assumes electrical periodicity and is directly applicable to reflectors and multistrip couplers. A modification is required in its application to transducers which is presently being developed [28].

The array of electrodes at the surface perturbs the boundary conditions so that both stress and charge distributions are induced at the surface. The basic problem is to determine these induced source distributions due to an incident surface wave; the perturbation theory developed in the last chapter (Eq. 5.23) is then used to determine the phase change of the incident wave and the generated reflected wave. The assumption, of course, is that the perturbation is small over a wavelength which is true in almost all useful applications.

In this chapter we will consider only piezoelectric scattering due to the induced charge distribution; the mechanical scattering due to the induced stress distribution is discussed separately in the next chapter. In strong piezoelectric materials like $LiNbO_3$ the scattering from thin electrodes is predominantly due to induced charges; but in weak piezoelectric materials like quartz the mechanical scattering is more important.

We consider an incident surface wave from the left on a periodic array of electrodes each of which is connected to ground through an impedance Z (Fig. 6.1). The electrical potential at the surface associated with the wave is taken as a measure of its amplitude,

$$\phi_s = \phi_+ e^{-j\beta_o z} \tag{6.1}$$

where β_o is the unperturbed wavenumber. ϕ_+ is the amplitude (complex) of the wave entering an electrode from the left. The wave leaving to the right has its amplitude changed by $\Delta\phi_+$. In addition a reflected wave of amplitude $\Delta\phi_-$ is generated to the left. $\Delta\phi_+$ and $\Delta\phi_-$ are obtained by integrating Eq. 5.23 over one period:

$$\Delta\phi_+ = \frac{Z_o}{2} \int_{-p/2}^{+p/2} D_y(z)\, e^{j\beta_o z} \tag{6.2a}$$

$$\Delta\phi_- = \frac{Z_o}{2} \int_{-p/2}^{+p/2} D_y(z)\, e^{-j\beta_o z} \tag{6.2b}$$

where, $Z_o = \dfrac{\phi_+ \phi_+^*}{2P_a}$

P_a being the power carried by a surface acoustic wave with a surface potential of ϕ_+.

To determine $D_y(z)$, we assume that an electrostatic field described by Poisson's equation is superposed on the piezoelectric field. The potential ϕ_e due to this field is written in a Fourier series from Floquet's theorem for periodic media:

$$\phi_e(y,z) = \sum_{n=-\infty}^{+\infty} \phi_n\, e^{-|\beta^{(n)}|y}\, e^{-j\beta^{(n)}z} \tag{6.3}$$

where, $\beta^{(n)} = \beta_o + n.\dfrac{2\pi}{p}$

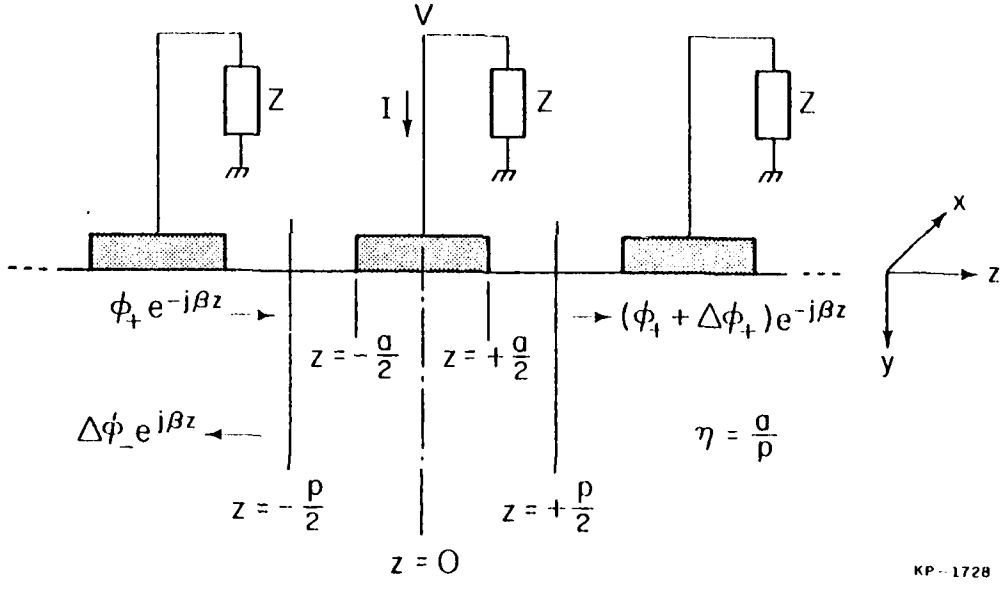

Figure 6.1: Reflection and transmission of surface acoustic waves at an electrode in a periodic array

The exponential decay along y follows from Laplace's equation for charge-free media.

The total electrical potential at the surface is given by,

$$\phi(z) = \phi_+ e^{-j\beta_o z} + \phi_e(y = 0, z) \tag{6.4}$$

The tangential electric field at the surface is obtained from the derivative of the potential:

$$E_z(z) = j\beta_o \phi_+ \, e^{-j\beta_o z} + \sum_{n=-\infty}^{\infty} j\beta^{(n)} \phi_n \, e^{-j\beta^{(n)} z} \tag{6.5a}$$

The electrostatic part of the field gives rise to a normal electric displacement $D_y(z)$ at the surface that is written from Laplace's equation:

$$D_y(z) = (\epsilon_p + \epsilon_o) \sum_{n=-\infty}^{\infty} |\beta^{(n)}| \, \phi_n \, e^{-j\beta^{(n)}} \tag{6.5b}$$

where ϵ_p is the effective permittivity of the substrate and ϵ_o is the permittivity of the medium above the surface. The problem now is to determine the ϕ_n's such that (Fig. 6.1)

$$E_z(z) = 0 \qquad |z| < \frac{a}{2} \tag{6.6a}$$

$$D_y(z) = 0 \qquad \frac{a}{2} < |z| < p/2 \tag{6.6b}$$

This is done analytically in [10] using the properties of the Legendre polynomial. Once the induced charges in the strips $D_y(z)$ is determined $\Delta\phi_+$ and $\Delta\phi_-$ are readily obtained from Eq. (6.2). A (3x3) matrix relating the fields at the two acoustic and one electrical ports (Fig. 6.2) is obtained analytically:

$$\begin{Bmatrix} \phi_- + \Delta\phi_- \\ \phi_+ + \Delta\phi_+ \\ I \end{Bmatrix} = \begin{bmatrix} A_{11} & A_{12} & A_{13} \\ A_{21} & A_{22} & A_{23} \\ A_{31} & A_{32} & A_{33} \end{bmatrix} \begin{Bmatrix} \phi_+ \\ \phi_- \\ V \end{Bmatrix} \tag{6.7}$$

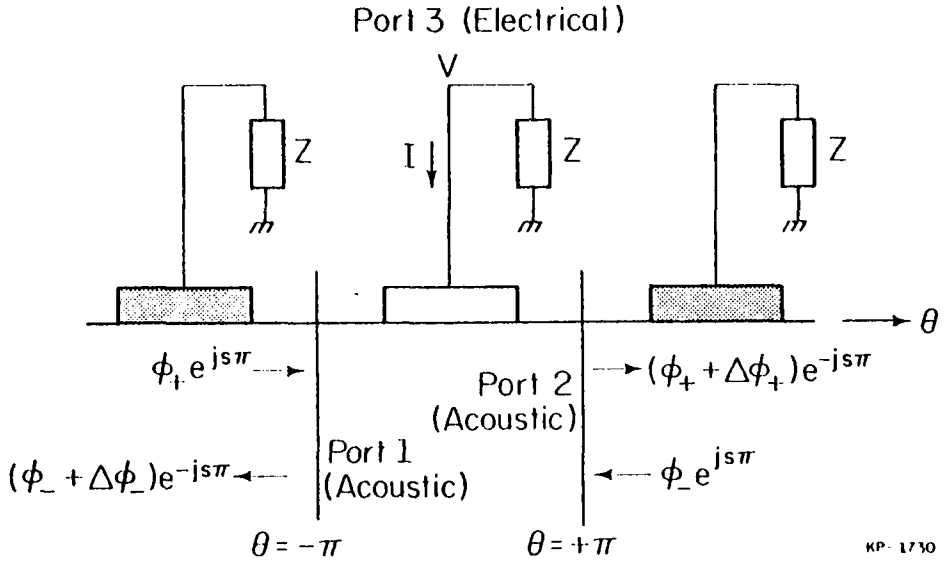

Figure 6.2: Scattering at an electrode in a periodic array

Fig. 6.2 is labeled in terms of dimensionless coordinates s and ϑ in place of β_o and z. In the above discussion we assumed a wave, Φ_+ incident from the left. The second column of the A-matrix corresponding to a wave, Φ_- incident from the right is obtained by symmetry.

The (2x2) scatter matrix, S, relating the two acoustic ports is easily obtained from the A-matrix by setting $I = V/Z$ where Z is the external load at each strip. Unconnected strips are described by $Z = \infty$ while shorted strips are described by $Z = 0$.

Thus a complete scatter matrix describing the piezoelectric scattering by a periodic array of electrodes is obtained analytically at all frequencies. The results have been applied to determine the reflection coefficient per strip at different stopbands and for different metalization ratios (= a/p). The details are described in [10].

Chapter 7: Mechanical Scattering from Periodic Arrays

In this chapter we consider the scattering due to a thin strip overlay of height h ($\ll$ wavelength) on the surface (Fig. 7.1a). An incident Rayleigh wave along a free surface induces normal and tangential stresses T^s_{xy}, T^s_{yy}, T^s_{zy} (Fig. 7.1b) at the interface between the strip and the surface. The basic problem is to determine these stresses in terms of the particle velocities of the incident wave; the stresses can then be used in the perturbation Eq. (5.23) to yield the phase shift of the incident wave and the reflected wave.

To a first approximation, we may assume that the strip floats on the wave so that the entire strip moves with the same particle velocities as the unperturbed surface. In this case the problem amounts to finding the forces that have to be exerted to the strip by the interface in order to move it with the same particle velocities v_x, v_y, v_z as the unperturbed surface. This is done by considering the forces acting on a differential element dxdz of the strip of height h. From the x-directed forces (Fig. 7.2a),

$$T^s_{xy} = j\omega\rho' h\, v_x - h.\, \frac{\partial T'_{xz}}{\partial z} \tag{7.1a}$$

From the y-directed forces (Fig. 7.2b),

$$T^s_{yy} = j\omega\rho' h\, v_y - h\, .\, \frac{\partial T'_{yz}}{\partial z} \tag{7.1b}$$

From the z-directed forces (Fig. 7.2c),

$$T^s_{zy} = j\omega\rho' h\, v_z - h.\, \frac{\partial T'_{zz}}{\partial z} \tag{7.1c}$$

where ρ' is the mass-density of the strip.

Eqs. (7.1) give the interface stresses in terms of the surface wave particle velocity provided we can express T'_{xz}, T'_{yz} and T'_{zz} in

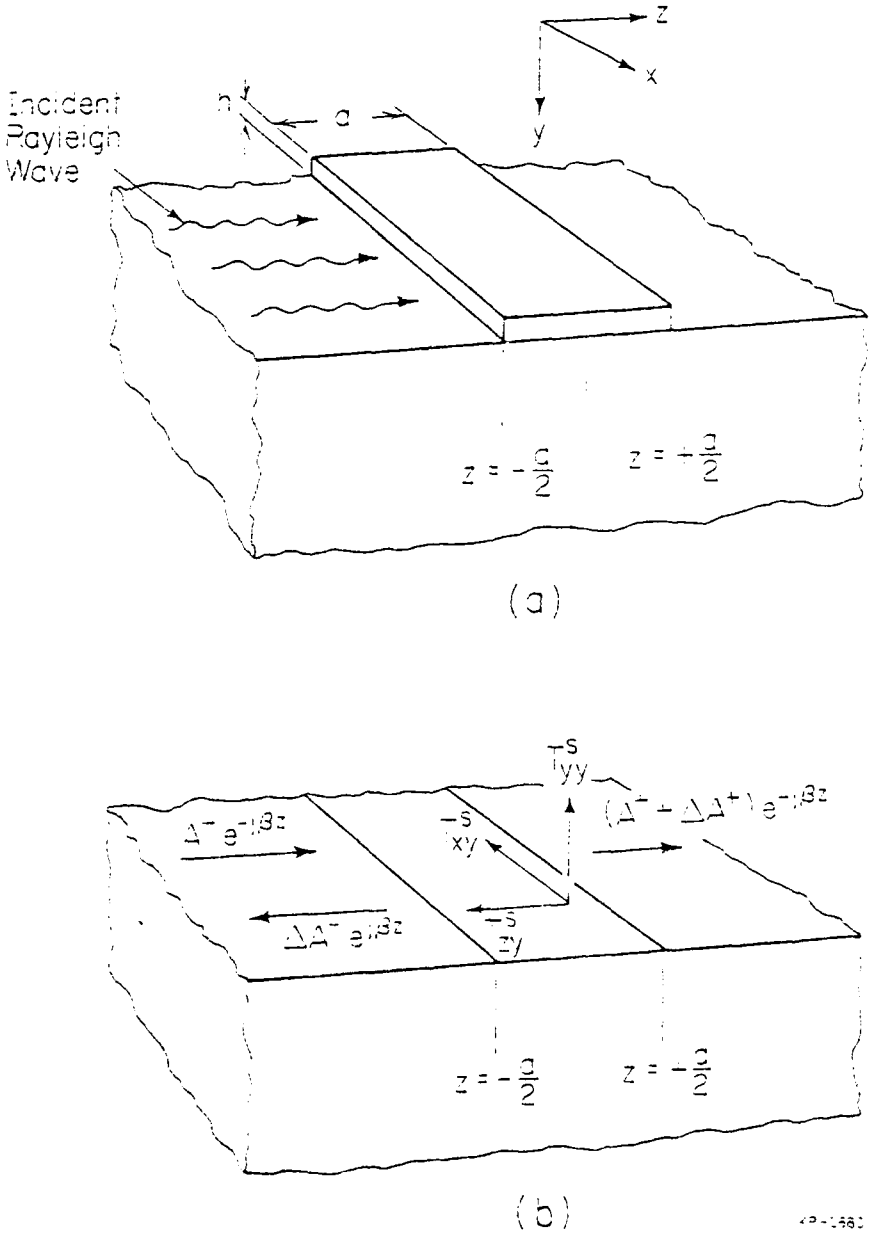

Figure 7.1: (a) Incident Rayleigh wave on a thin strip overlay
(b) Generation of a reflected wave by stresses induced at the strip-substrate interface

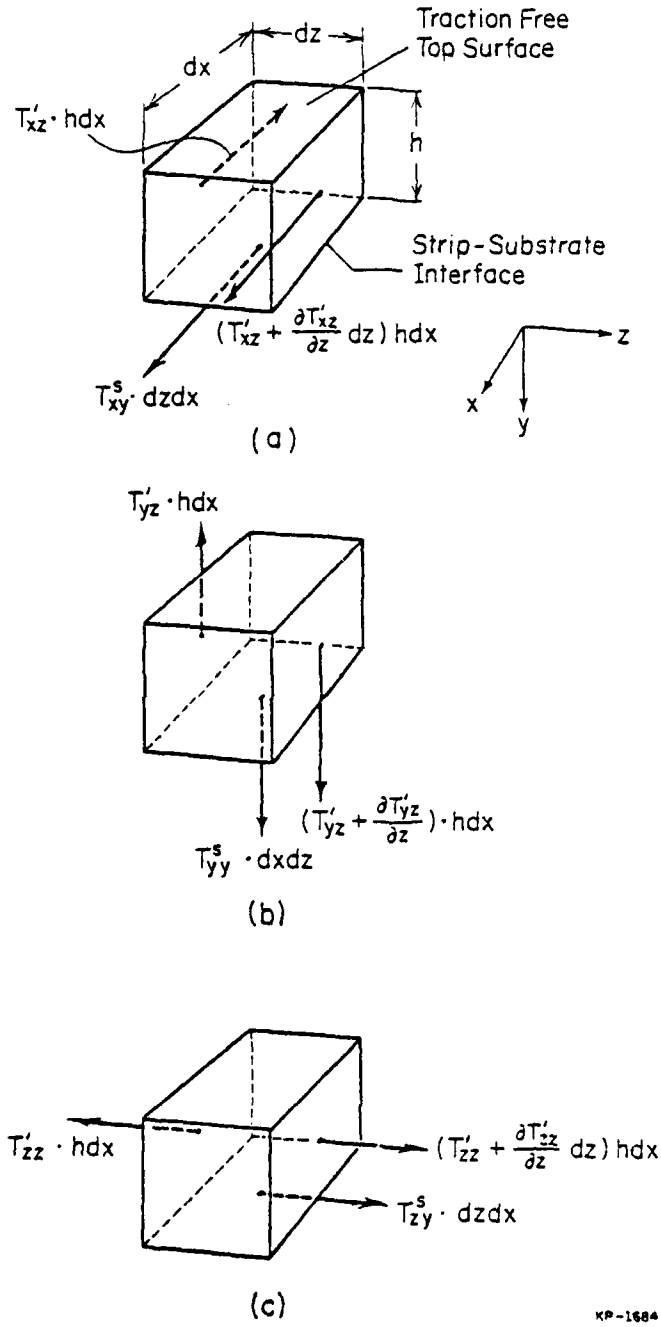

Figure 7.2: First order forces acting on a differential element of the strip in
(a) x-direction
(b) y-direction
(c) z-direction

terms of v_x, v_y, v_z. This is done approximately from the plane strain equations to yield [30],

$$T'_{xz} = - \frac{1}{C_s} \mu' v_x \tag{7.2a}$$

$$T'_{zz} = - \frac{1}{C_s} \frac{4\mu'(\lambda' + \mu')}{\lambda' + 2\mu'} \tag{7.2b}$$

$$T'_{yz} = 0 \tag{7.2c}$$

where C_s is the surface wave velocity and λ', μ' are the Lamé constants of the strip material. For anisotropic strips, similar equations are derived but are more complicated.

So far we have not considered the effect of the finite strip width. At the edges of the strip ($z = \pm a/2$) the situation changes somewhat from that depicted in the force diagrams of Fig. 7.2. There is no strip material on one side to exert the stresses T'_{xz}, T'_{yz} and T'_{zz} on the z- face of the strip. So in order to keep the strip vibrating with the same particle velocities, the substrate has to exert extra forces at the edges to make up for the missing material to the left at $z = - a/2$ and to the right at $z = + a/2$.

The interface stresses thus have the spatial distribution shown in Fig. 7.3. The stresses are uniform under the strip with delta functions at the two edges. In the figure $\alpha'_x = \mu'$ and $\alpha'_z = \frac{4\mu'(\lambda' + \mu')}{\lambda' + 2\mu'}$.

Using these stress distributions the reflection coefficients predicted for several practical cases agree well with measured values. The details are described in [11]. It is found, however, that this does not predict the slight lowering of phase velocity from the unperturbed value that is experimentally observed. The physical reason for this velocity

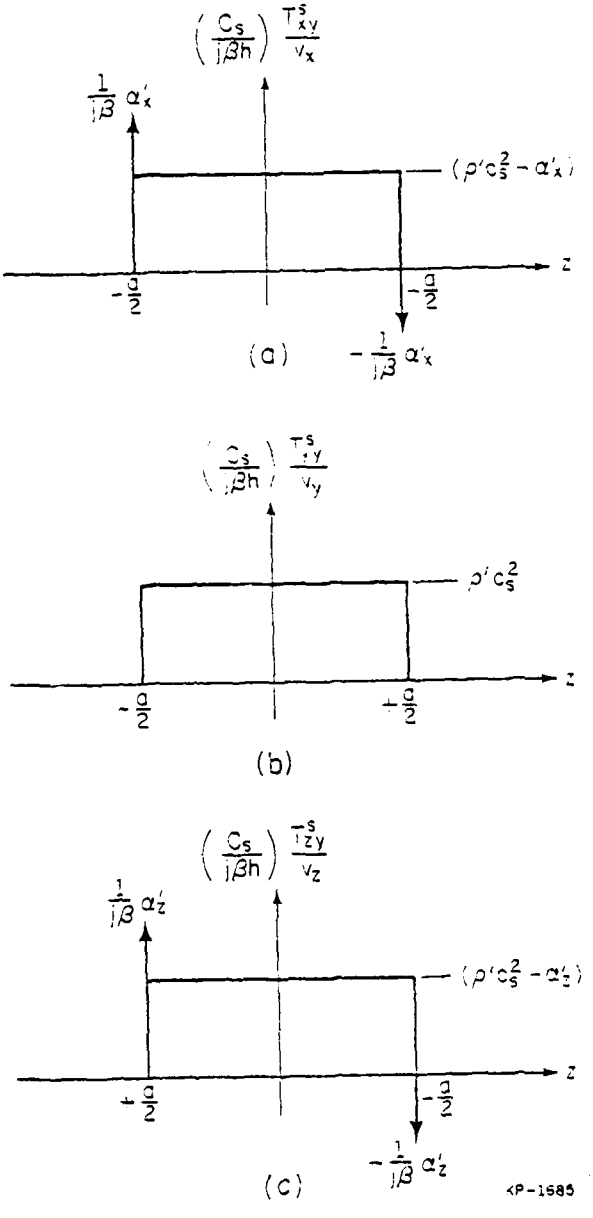

Figure 7.3: Spatial distribution of
(a) x-directed interface stresses
(b) y-directed interface stresses
(c) z-directed interface stresses

lowering is that, due to the interface stresses, the substrate is distorted somewhat, and the assumption of the strips floating on the wave made here is not strictly true. This distortion represents a relaxation of the system causing a lowering in velocity. Mathematically, this is taken into account by assuming the excitation of evanescent modes that store energy.

The first-order stress shown in Fig. 7.3 induces particle displacements with spatial harmonics separated from the unperturbed wavenumber β by an integer multiple of $2\pi/p$ where p is the period (Floquet's Theorem) of the array. These fields store energy and their effect on the incident wave velocity is obtained from (5.23) using the second-order stress generated by the induced particle displacement field. A complete analysis of this stored energy effect is described in [12]; the phase velocity and reflection are correctly predicted using this analysis.

The analysis described in this chapter yields the mechanical part of the scatter matrix of an electrode in a periodic array. These are added to the A_{11}, A_{12}, A_{21}, A_{22} obtained in chapter 6 (Eq. 6.7) for the piezoelectric part of the scattering. The other matrix elements are, however, unchanged by mechanical effects.

Chapter 8: Multistrip Couplers

A multistrip coupler (MSC) is a periodic array of electrodes that is used to couple from one surface wave track to another (Fig. 8.1). Each strip of the MSC samples the potential of the incoming acoustic wave and applies it to all the tracks generating acoustic waves in each track. Because of the traveling wave nature of the excitation, the generated waves are unidirectional; reverse waves may be ignored outside the stopbands. MSC's are widely used in surface wave technology as track-changers, beam compressors and couplers.

In this chapter we will derive the (MxM) scatter matrix of a single strip in a MSC that relates the incoming and outgoing acoustic waves in the M tracks (Fig. 8.2)

$$A_i^n = \sum_{k=1}^{M} b_{ik}^n B_k^n \qquad , i = 1, M \tag{8.1}$$

where B_k^n is the incoming wave amplitude in the k^{th} track at the n^{th} strip and A_i^n is the outgoing wave amplitude in the i^{th} track at the n^{th} strip. We wish to determine b_{ik}. The superscript n denoting strip number is dropped for convenience. The scatter matrix of successive strips can then be cascaded to obtain the scattering characteristics of the coupler as a whole.

Neglecting backward waves, we may write in terms of the A-matrix in chapter 6,

$$A_i = A_{21}^{(i)} B_i + A_{23}^{(i)} V \tag{8.2a}$$

$$I_i = A_{31}^{(i)} B_i + A_{33}^{(i)} V \qquad , i = 1, M \tag{8.2b}$$

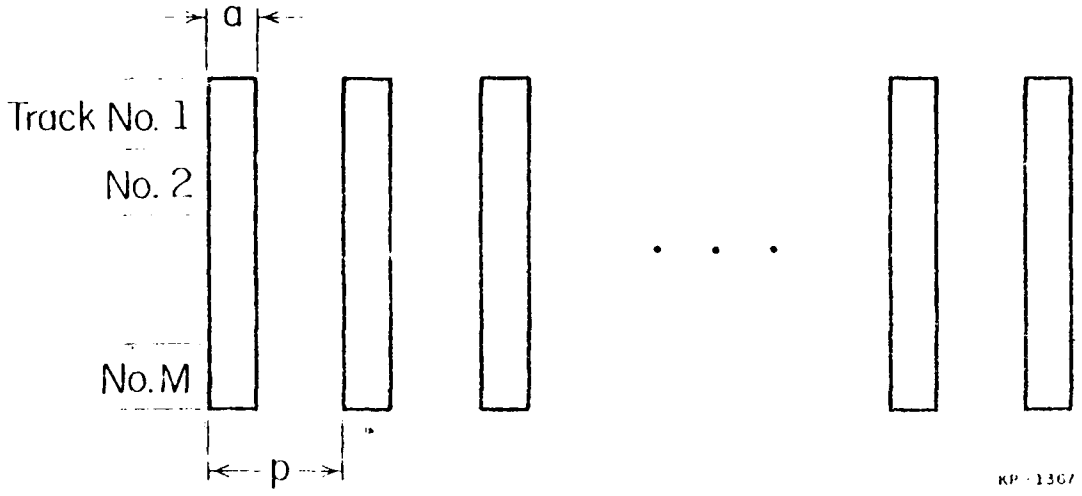

Figure 8.1: A multistrip-coupler with M tracks

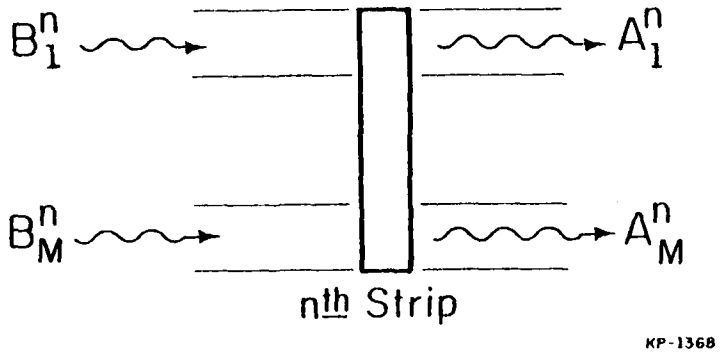

Figure 8.2: Incoming and outgoing waves in M tracks of the n^{th} strip

where I_i is the current into the i^{th} track, V is the common voltage of all the tracks, and $A_{mn}^{(i)}$ represents the A-matrix elements of the i^{th} track.

If a load Y_L is connected externally to each strip then,

$$\sum_{i=1}^{M} I_i + VY_L = 0 \tag{8.3}$$

Using I_i from (8.2b) in (8.3),

$$\sum_{i=1}^{M} A_{31}^{(i)} B_i + V \cdot \left[Y_L + \sum_{i=1}^{M} A_{33}^{(i)} \right] = 0$$

So that, $$V = - \frac{\sum_{i=1}^{M} A_{31}^{(i)} B_i}{Y} \tag{8.4a}$$

where $$Y = Y_L + \sum_{i=1}^{M} A_{33}^{(i)} \tag{8.4b}$$

Using (8.4a) in (8.2a),

$$A_i = A_{21}^{(i)} B_i - \frac{A_{23}^{(i)}}{Y} \sum_{k=1}^{M} A_{31}^{(k)} B_k \tag{8.5}$$

Comparing with (3.1) we have the scatter matrix b_{ik}:

$$b_{ik} = A_{21}^{(i)} \delta_{ik} - \frac{A_{23}^{(i)} A_{31}^{(k)}}{Y} \tag{8.6}$$

where $\delta = 1 \qquad i = k$

$\delta = 0 \qquad i \neq k.$

The first term in (8.6) denotes the direct propagation while the second term denotes coupling from other tracks. An incident wave in track k produces a current proportional to $A_{31}^{(k)}$. The strip voltage is related to the current by the total strip admittance Y. The strip voltage is then proportional to $A_{31}^{(k)}/Y$ which generates a wave in track i proportional to $A_{23}^{(i)} A_{31}^{(k)}/Y$.

A simple circuit model for the scatter matrix is described in [13]. The scatter matrix method is applicable to the analysis of non-uniform couplers with slowly varying characteristics; such couplers are not amenable to analysis by conventional techniques. Details of this technique with examples are described in Reference [13].

Chapter 9: A Unified Theory of Transducers

In the last three chapters we have discussed the scatter matrix for a single strip in a periodic array. As mentioned earlier, this formulation is directly applicable to reflectors and multistrip couplers; but modifications are necessary to apply it to transducers which are usually not electrically periodic. A complete scatter matrix description for transducers is presently being developed [28].

The scatter matrix approach to transducers, though accurate, requires numerical implementation thus lending little physical insight. A less accurate approach known as the "weak coupling approximation" has the advantage of yielding simple results that are easily interpreted physically. The acoustic waves generated by the transducer induce charges in the electrodes which in turn regenerate acoustic waves. This regeneration is neglected in the weak-coupling approximation. With this approximation, the charge distribution in the array is calculated from electrostatics alone. The problem then divides into two steps:

(1) The charge distribution on the electrodes is determined from the electrostatic equation.

(2) The calculated charge distribution is used in Eq. (5.23) to determine the generated acoustic waves.

This chapter describes the second step in terms of an aribtrary charge distribution. The next chapter discusses the first step for SAW interdigital transducers.

In this chapter we will discuss the radiation conductance, capacitance and Q of the generalized transducer depicted in Fig. 9.1. These results are universal and can be applied to the excitation of any acoustic mode (SAW or LAW); certain unifying features common to all transducers are

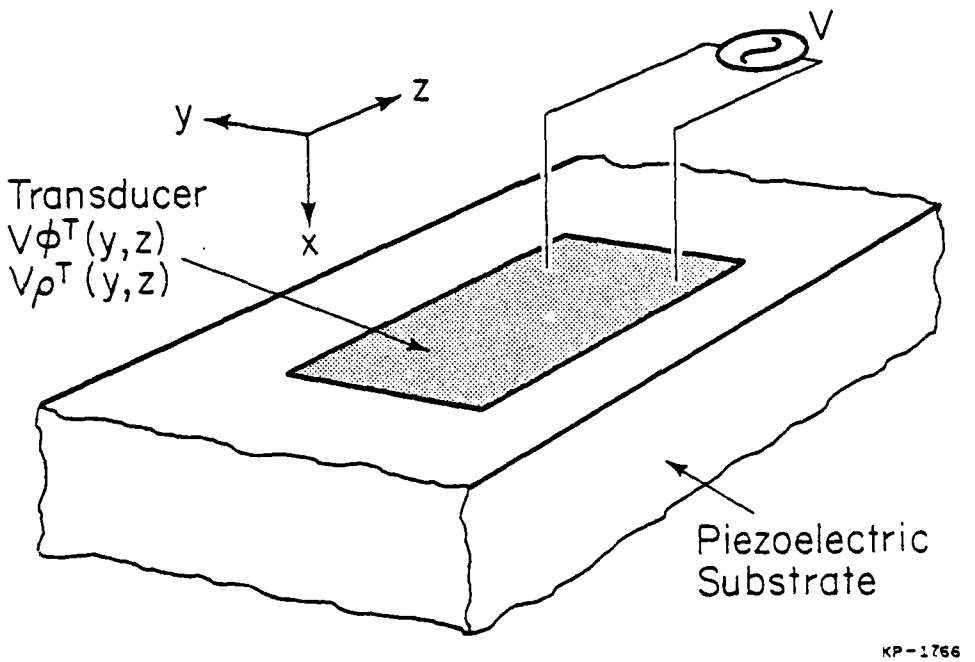

Figure 9.1: A generalized transducer producing a potential distribution $V\phi^T$ and a charge distribution $V\rho^T$ proportional to the terminal voltage V

revealed through this general formulation. An external generator impresses an alternating voltage V at a frequency ω across the terminals of the transducer which is an interconnected pattern of electrodes that produces a potential distribution on the surface given by $V\phi^T(y,z)$. The function $\phi^T(y,z)$ is characteristic of the transducer and has to be determined from the electrostatic equations as discussed earlier. Corresponding to this potential distribution we have a charge distribution per unit area in the transducer $V\rho^T(y,z)$. The peak electrostatic energy, W^T, stored in the transducer is given by,

$$W^T = \frac{V^2}{2} \langle \phi^T | \rho^T \rangle \tag{9.1a}$$

$$\text{where } \langle \phi^T | \rho^T \rangle = \iint_{\substack{\text{over the} \\ \text{transducer}}} dydz \; \phi^{T*}(y,z) \; \rho^T(y,z) \tag{9.1b}$$

Since the peak energy in a capacitor is given by $\frac{1}{2}CV^2$, the capacitance of the transducer C^T is obtained as

$$C_T = \langle \phi^T | \rho^T \rangle \tag{9.2}$$

Now, let us obtain the radiation conductance of the transducers due to the generation of any particular acoustic mode. Suppose this mode has an electrical potential at the surface given by $A\phi^L(y,z)$ where A is the amplitude of the wave. The total power carried by the mode is written as $|A|^2.P_L$. We then have from equation (5.23),

$$\frac{dA}{A} = \frac{A^* V \int dy \; \phi^{L*}(y,z) \; j\omega \; \rho^T(y,z)}{4.|A|^2 P_L} \tag{9.3}$$

If we assume the wave grows from zero amplitude to a finite amplitude A_0 over the length of the transducer, then A_0 is obtained by integrating (9.3):

$$A_0 = \frac{j\omega V}{4P_L} \langle \phi^L | \rho^T \rangle \tag{9.4}$$

where $\langle \phi^L | \rho^T \rangle$ is defined analogous to (9.1b). The radiated acoustic power, P_a, is then written as,

$$\begin{aligned} P_a &= |A_0|^2 . P_L \\ &= \frac{\omega^2 V^2}{16 P_L} \cdot |\langle \phi^L | \rho^T \rangle|^2 \end{aligned} \tag{9.5}$$

This is the power coupled to one mode in one direction only. There will, in general, be some power coupled to the wave in the other direction, as well as to other modes. The same expression (9.5) will hold with the appropriate ϕ^L and P_L.

Since the power dissipated in a conductance G_L is given by $\frac{1}{2} G_L V^2$ we may write from (9.5),

$$G_L = \frac{\omega^2}{8P_L} |\langle \phi^L | \rho^T \rangle|^2 \tag{9.6}$$

Here G_L represents the power radiated into <u>one mode</u> in <u>one direction</u> only. The expression G_L may be written in terms of the fractional changes in velocity of the acoustic mode caused by completely shorting the surface with a conducting layer. Suppose that a charge $-A.\rho^L(y,z)$ per unit area is induced on the conducting layer by the acoustic wave of amplitude A. Then we can show from (5.23) that,

$$\left| \frac{\Delta v}{v} \right| = \frac{\omega}{4P_L} \cdot \frac{1}{\beta_0} \int dy \; \phi^{L*}(y,z) \; \rho^L(y,z) \tag{9.7}$$

where β_0 is the unperturbed wavenumber of the acoustic mode. Now for a travelling wave $\phi^L(y,z)$ depends on z through an exponential phase factor $\exp(-j\beta_0 z)$. The charge induced on a uniform conducting sheet also has the same phase factor so that $\phi^{L*}(y,z)\rho^L(y,z)$ is independent of z. We can then

write,

$$\int dy\ \phi^{L*}(y,z)\ \rho^{L}(y,z) = \frac{1}{L}\ \langle \phi^{L} | \rho^{L} \rangle \tag{9.8}$$

where L is the length of the transducer and $\langle \phi^{L} | \rho^{L} \rangle$ is defined as in (9.1b).

Using (9.7) and (9.8) the radiation conductance is written as,

$$G_L = \frac{\omega}{2} \cdot \left|\frac{\Delta v}{v}\right| \cdot (\beta_0 L) \cdot \frac{|\langle \phi^{L} | \rho^{T} \rangle|^2}{\langle \phi^{L} | \rho^{L} \rangle} \tag{9.9}$$

We now have the radiation conductance and capacitance of the generalized transducer. It will be noted here that if more than one acoustic mode is coupled to the transducer then G_L is computed similarly for each mode all the conductances are placed in parallel. Assuming only one mode we have for Q,

$$Q = \frac{\omega C_T}{G_L} = \frac{2\langle \phi^{T} | \rho^{T} \rangle\ \langle \phi^{L} | \rho^{L} \rangle}{\left|\frac{\Delta v}{v}\right| \cdot (\beta_0 L) \cdot |\langle \phi^{L} | \rho^{T} \rangle|^2}$$

$$= \frac{2}{\pi K^2 N} \cdot \frac{\langle \phi^{T} | \rho^{T} \rangle \cdot \langle \phi^{L} | \rho^{L} \rangle}{|\langle \phi^{L} | \rho^{T} \rangle|^2} \tag{9.10}$$

where $K^2 = 2\left|\frac{\Delta v}{v}\right|$

and N is number of wavelengths in the transducer = $\frac{L}{\lambda}$

The other terms are redefined here for convenience:

(1) $\langle \phi | \rho \rangle = \iint_{\text{over the transducer}} dydz\ \phi^{*}(y,z)\ \rho(y,z)$

(2) $\phi^{T}(y,z)$ and $\rho^{T}(y,z)$ are the potential and charge distributions produced by the transducer with unit voltage across its terminals.

(3) $\phi^{L}(y,z)$ is the potential distribution of a unit amplitude acoustic mode along a free surface.

(4) $-\rho^L(y,z)$ is the induced charge due to a unit amplitude acoustic mode when the surface is shorted with a thin conductor. The minus sign is included in this definition because we may consider this charge as producing an electrostatic potential that exactly cancels the acoustic potential $\phi^L(y,z)$. Clearly then $+\rho^L$ is related to ϕ^L in the same way as ρ^T is related to ϕ^T, namely through the Poisson's equation.

In fact ϕ^T and ρ^T or ϕ^L and ρ^L are related through a convolution product:

$$\rho(y,z) = C(y,z) * \phi(y,z) \tag{9.11a}$$

where $C(y,z)$ represents the charge distribution due to a delta function of potential at y=0, z=0. Clearly the Fourier transforms are related by:

$$\bar{\rho}(k_y,k_z) = \bar{C}(k_y,k_z) \cdot \bar{\phi}(k_y,k_z) \tag{9.11b}$$

where the bars denote Fourier transforms and k_y,k_z are the spatial frequencies corresponding to y and z.

Now we can see from equation (9.10) that if $\phi^T = \phi^L$, that is, if the transducer produces a potential distribution that exactly matches that due to the acoustic mode, then,

$$Q = \frac{2}{\pi K^2 N}$$

We can readily show that this is really the minimum possible Q and represents an optimally coupled transducer so that the factor

$$F = \frac{Q_{min}}{Q} = \frac{|\langle \phi^L | \rho^T \rangle|^2}{\langle \phi^T | \rho^T \rangle \cdot \langle \phi^L | \rho^L \rangle} \tag{9.12}$$

may be taken as a measure of the efficiency of the transducer structure. To see that $F < 1$ for any $\phi^T \neq \phi^L$ we note that the integration of space

variables over y,z can be replaced by an integration of the Fourier transforms over k_y, k_z, so that using (9.11b),

$$F = \frac{|\langle \bar{\phi}^L | \bar{C}\ \bar{\phi}^T \rangle|^2}{\langle \bar{\phi}^T | \bar{C}\ \bar{\phi}^T \rangle \cdot \langle \bar{\phi}^L | \bar{C}\ \bar{\phi}^L \rangle} \tag{9.13a}$$

where $\langle\ \rangle$ now denotes integration over k_y, k_z and the bars denote respective Fourier transforms. The two terms in the denominator are the norms of $\bar{\phi}^T$ and $\bar{\phi}^L$ with a weight function $\bar{C}$ while the numerator is the inner product of $\bar{\phi}^L$ and $\bar{\phi}^T$ with a weight function $\bar{C}$. Clearly F is maximum when the inner product is maximum, that is, when $\bar{\phi}^L = \bar{\phi}^T$. This is, of course, what one would expect intuitively. We note here that F can be written in terms of charges as well:

$$F = \frac{|\langle \bar{\rho}^L\ \bar{C}^{-1} | \bar{\rho}^T \rangle|^2}{\langle \bar{\rho}^T\ \bar{C}^{-1} | \bar{\rho}^T \rangle\ \langle \bar{\rho}^L\ \bar{C}^{-1} | \bar{\rho}^L \rangle} \tag{9.13b}$$

The quantity F is a good figure of merit for a transducer exciting a certain acoustic mode. As an illustration let us evaluate it for a SAW interdigital transducer with alternating polarities. Since the SAW is uniform along y, we may neglect the integrations over y (or k_y). Also we note that for fields uniform along y,

$$\bar{C}(k_y = 0,\ k_z) = \epsilon_p |k_z| \tag{9.14}$$

where ϵ_p is the effective permittivity of the substrate. This is shown readily from Poisson's equation.

Suppose the transducer potential distribution is periodic with a Fourier series representation to the form:

$$\phi^T(z) = \sum_{n=-\infty}^{\infty} \bar{\phi}_n^T\ e^{-jn\beta_0 z} \tag{9.15}$$

where β_0 is equal to the wavenumber of the acoustic mode being excited.

$$\phi^L(z) = \phi^L(0)\ e^{-j\beta_0 z} \tag{9.16}$$

Using (9.14), (9.15) and 9.16) we obtain C_T from (9.2), G_a from (9.9) and F from (9.13a):

$$C_T = \langle \bar{\phi}^T | \bar{C}\ \bar{\rho}^T \rangle$$

$$= 4\pi\epsilon_p N \sum_{n=-\infty}^{\infty} n |\bar{\phi}_n^T|^2 \tag{9.17a}$$

$$G_a = 2G_L = \frac{\omega}{2} \left|\frac{\Delta v}{v}\right| 4\pi N \ \frac{|\langle \bar{\phi}^L | \bar{C}\ \bar{\phi}^T \rangle|^2}{\langle \bar{\phi}^L | \bar{C}\ \bar{\phi}^L \rangle}$$

$$= \left|\frac{\Delta v}{v}\right| \omega\epsilon_p 4\pi^2 N^2\ |\bar{\phi}_1^T|^2 \tag{9.17b}$$

$$F = \frac{|\bar{\phi}_1^T|^2}{\sum_{n=0}^{\infty} n|\bar{\phi}_n^T|^2} = .91 \tag{9.17c}$$

Here the Fourier transform versions of (9.2) and (9.9) for C_T and G_a have been used and the summation from $-\infty$ to $+\infty$ has been replaced by twice the summation from 0 to $+\infty$ assuming $\bar{\phi}_n^T = \bar{\phi}_{-n}^T$. Also G_a has been multiplied by 2 to account for the bidirectionality. The numerical value of F was computed using the potential distribution for a SAW IDT with alternating polarities and with equal electrodes and gaps..

It is evident that while the capacitance arises from all the Fourier components of the transducer distribution function ϕ^T, the conductance comes only from the Fourier component that matches the acoustic wave being excited. The Q is thus minimized when ϕ^T contains only one Fourier component matching the acoustic wave, that is, when $\phi^T = \phi^L$.

The equations derived in this chapter are applied readily to line waves as well. However, for any given transducer we have to obtain

the transducer distribution function $\mathfrak{p}^T$ by solving the electrostatic Poisson's equation with the appropriate surface boundary conditions. The line wave distribution $\mathfrak{p}^L$ is obtained from the field equations as discussed in Chapter 3. Fig. 3.4 shows $\mathfrak{p}^L$ for the particular wedge used in our experiments.

The problem of obtaining $\mathfrak{p}^T$ for the line wave transducers is a three dimensional electrostatic field problem and unfortunately this has not been solved for the single phase or the triangular transducer discussed in Chapter 3. However, remembering that the optimum transducer is one with $\mathfrak{p}^L = \mathfrak{p}^T$, we can get a feel for the relative Q's of different types of transducers.

The transducer distribution $\mathfrak{p}^T$ should match the line wave distribution $\mathfrak{p}^L$ both along the propagation direction and in the transverse direction. Interdigital transducers provide a fairly good match for the propagation direction as shown by the high F computed for SAW for an interdigital transducer. However, it is uniform in the transverse direction and is not a good match for the LAW distribution (Fig. 3.4). In fact, the F computed for LAW for a 1λ wide IDT is $\sim .15$ showing rather poor efficiency. The sawtooth transducer is similar to the IDT but the fundamental Fourier component is weighted across the beam and can be matched to the LAW distribution to provide a higher F. However, no quantitative calculation has been carried out.

The single phase transducer is clearly the weakest because it provides a poor match even in the propagation direction. Since there are no negative electrodes between the positive electrodes the potential is not forced to alternate along the propagation path so that the fundamental Fourier component is rather small.

The condition for optimum coupling $\phi^T = \phi^L$ suggests that the transducer in Fig. 9.2 should be fairly efficient. However, it is difficult to implement because of the cross-overs needed to make connections to the electrodes.

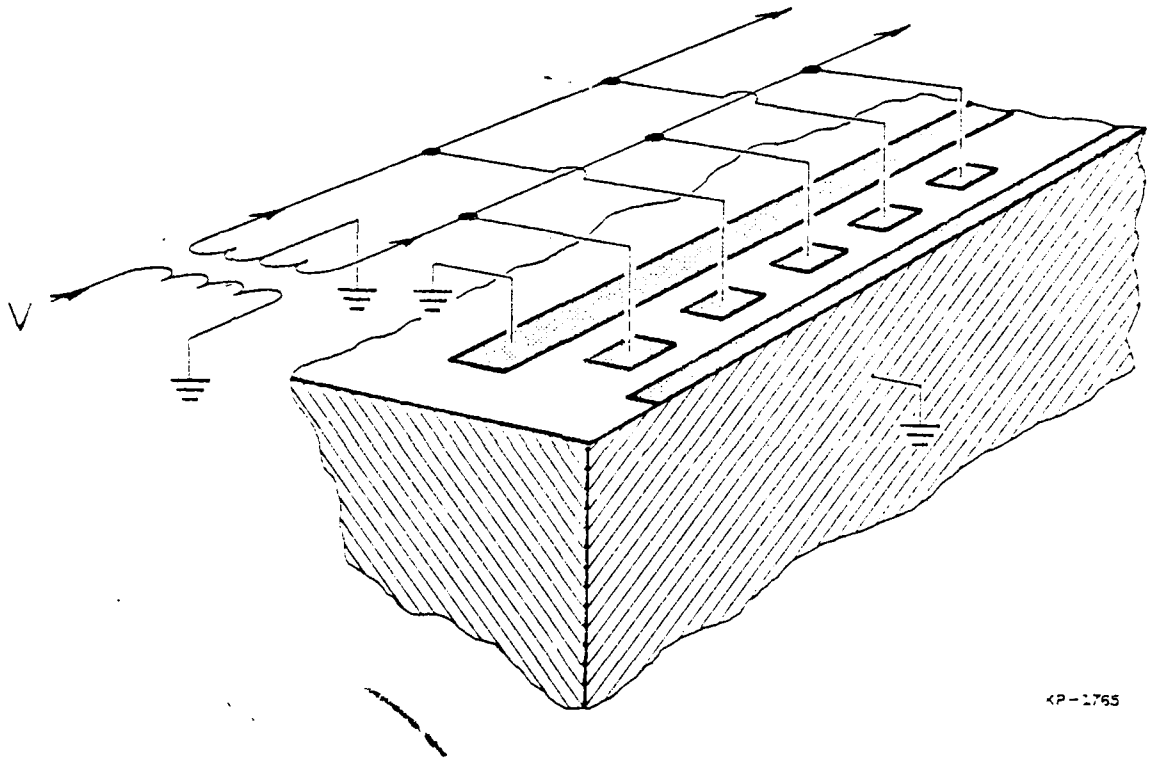

Figure 9.2: A conceptual LAW transducer for good coupling

Chapter 10: The Superposition Principle as Applied to Transducer Analysis and Design

In this chapter we consider an interdigital transducer consisting of a periodic array of electrodes with a specified voltage sequence (Fig. 10.1). As mentioned in the last chapter, the generation of surface waves by the transducers is computed in two steps. First, the charge distribution on the electrodes is determined assuming the substrate to be a pure dielectric. The calculated charge distribution is then used in Eq. (5.23) to determine the waves generated in either direction. Here we will describe an application of the superposition principle that simplifies the first step considerably for periodic SAW interdigital transducers. This first step of the problem requires us to solve the electrostatic equations so that the charge is zero in the gaps and the electrical potential has the specified values on the electrodes. This is a non-trivial problem especially for arbitrary electrode voltages. Moreover, the problem has to be solved anew for each new set of voltages.

In this chapter we will show that the charge distribution in a periodic transducer is written as a convolution product of the electrode voltages with a basic charge distribution that depends only on the electrode metalization ratio (=a/p), so that it is not necessary to solve the field equations for each new set of voltages.

Consider the transducer in Fig. 10.2 (a) with 1V applied to the central electrode and all other electrodes grounded. The charge distribution in this array $\sigma(x)$ (Fig. 10.2 (b)) is the basic charge distribution mentioned earlier. To show this let us consider the three cases shown in Fig. 10.3. In Fig. 10.3 (a) the charge distribution is clearly $V_0\sigma(x)$. In Fig. 10.3 (b) the charge distribution is $V_1\sigma(x-p)$. Now, in Fig. 10.3 (c) the

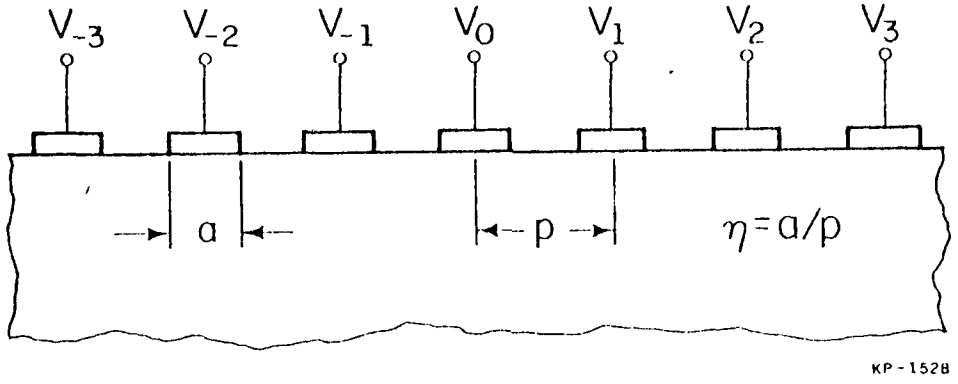

Figure 10.1: A periodic transducer with arbitrary voltages

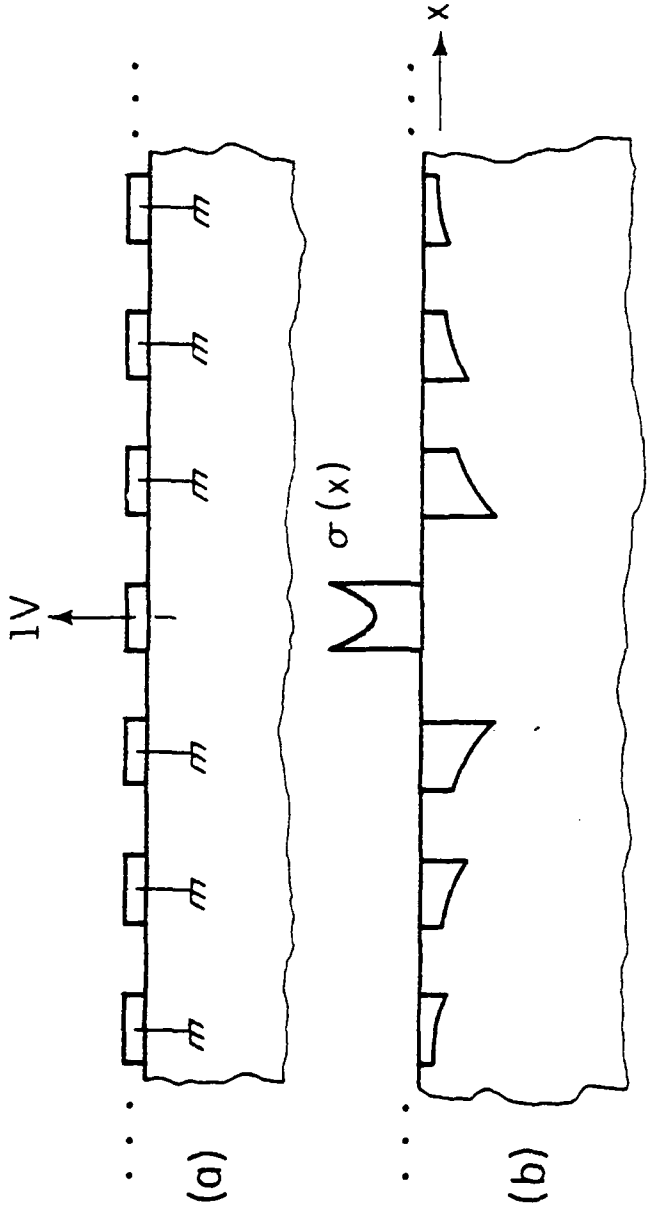

Figure 10.2: Single tap transducer
(a) Electrode voltages
(b) Charge distribution

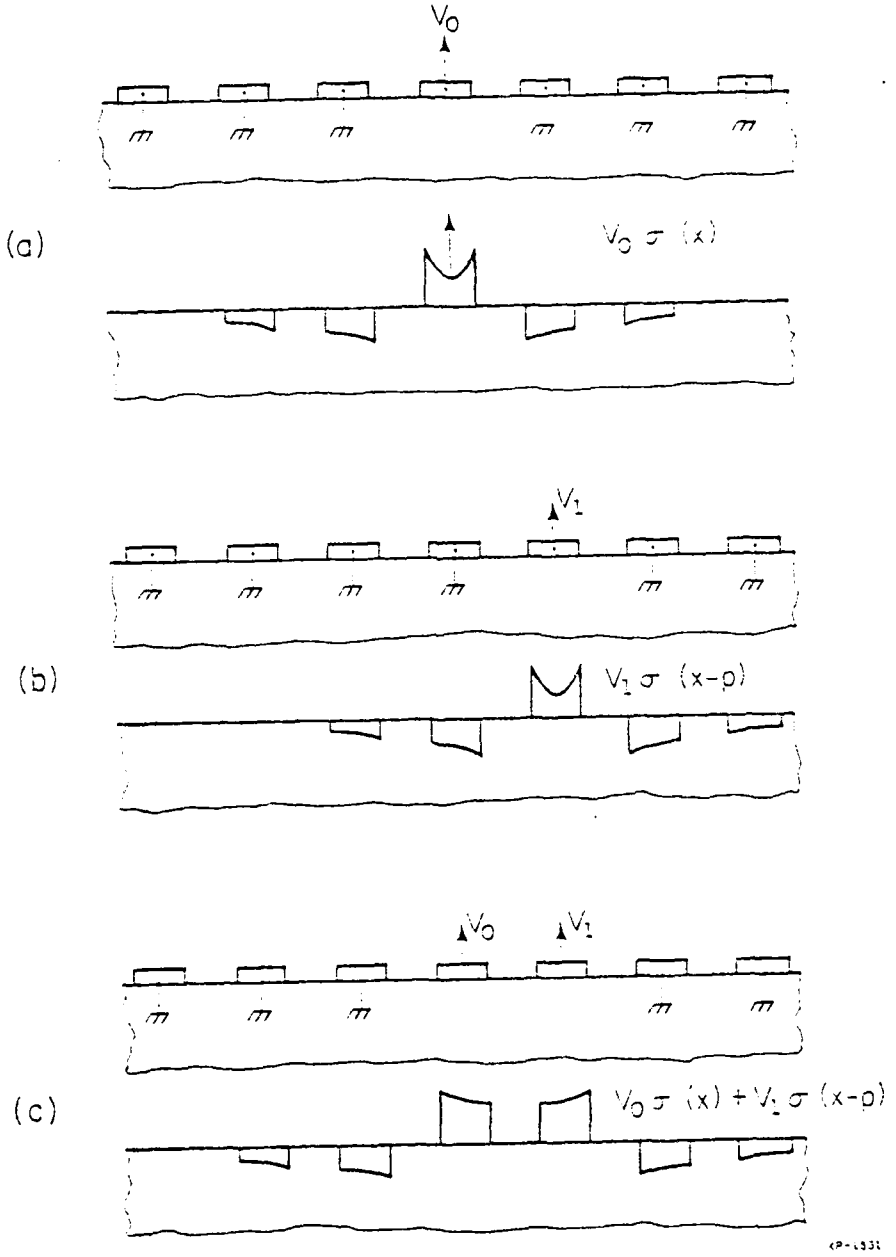

Figure 10.3: Charge distribution in a periodic transducer as a superposition of basic charge distribution functions

the charge distribution is obtained by superposing the charge distributions in Figs. 10.3 (a) and 10.3 (b) giving $V_0\sigma(x) + V_1\sigma(x-p)$. This is true because the field equations are linear and the sum of two solutions is also a valid solution. The only question is whether it has the correct boundary values. It is easy to check that it does.

Similarly for an arbitrary sequence of voltages as in Fig. 10.1 we may write the charge distribution Q(x) as,

$$Q(x) = \sum_n V_n \sigma(x - np) \tag{10.1a}$$

$$= V(x) * \sigma(x) \tag{10.1b}$$

where $$V(x) = \sum_n V_n \delta(x - np) \tag{10.1c}$$

and the * denotes convolution. It will be noted that this argument is exact only for an infinite array of electrodes with all electrodes occurring periodically. The end effects are easily accounted for by adding a few grounded electrodes at each end since the effects of neighboring electrodes are negligible beyond the third nearest neighbor. However, if any electrodes are withdrawn from the array (as is true for a few practical transducers) then this analysis is not applicable in its present form.

It can be shown from the perturbation equation (5.23) that the total surface wave amplitude, A_S at a frequency ω generated by a distributed charge distribution Q(x) proportional to the Fourier transform of the charge distribution at a spatial harmonic equal to the wavenumber of the surface wave. Thus,

$$A_S(\omega) \propto \bar{Q}(k = \omega/v_S) \tag{10.2}$$

where $\bar{Q}(k)$ is the Fourier transform of Q(x)

and v_S = surface wave velocity.

From (10.1) we then have,

$$A_S(\omega) \propto \bar{V}(k = \omega/v_s) \cdot \bar{\sigma}\left(k = \frac{\omega}{v_s}\right) \tag{10.3}$$

where $\bar{V}(k)$ and $\bar{\sigma}(k)$ are the Fourier transforms of $V(x)$ and $\sigma(x)$. The overall response thus splits into the product of an array factor $\bar{V}(k)$ with an element factor $\bar{\sigma}(k)$. The array factor is obtained from a simple Fourier transformation of the electrode voltages while the element factor is obtained once and for all from field theory. Fig. 10.4 shows the element factor $k^{1/2}\,\bar{\sigma}(k)$ plotted against k for various values of the metallization ratio. These plots were obtained from field theory [18].

This concept has been applied to various types of transducers and the details are described in [15], [16], and [17]. Presently the technique is being extended to non-periodic transducers [29]. The principle is also being incorporated into a general scatter-matrix characterization of transducers [28].

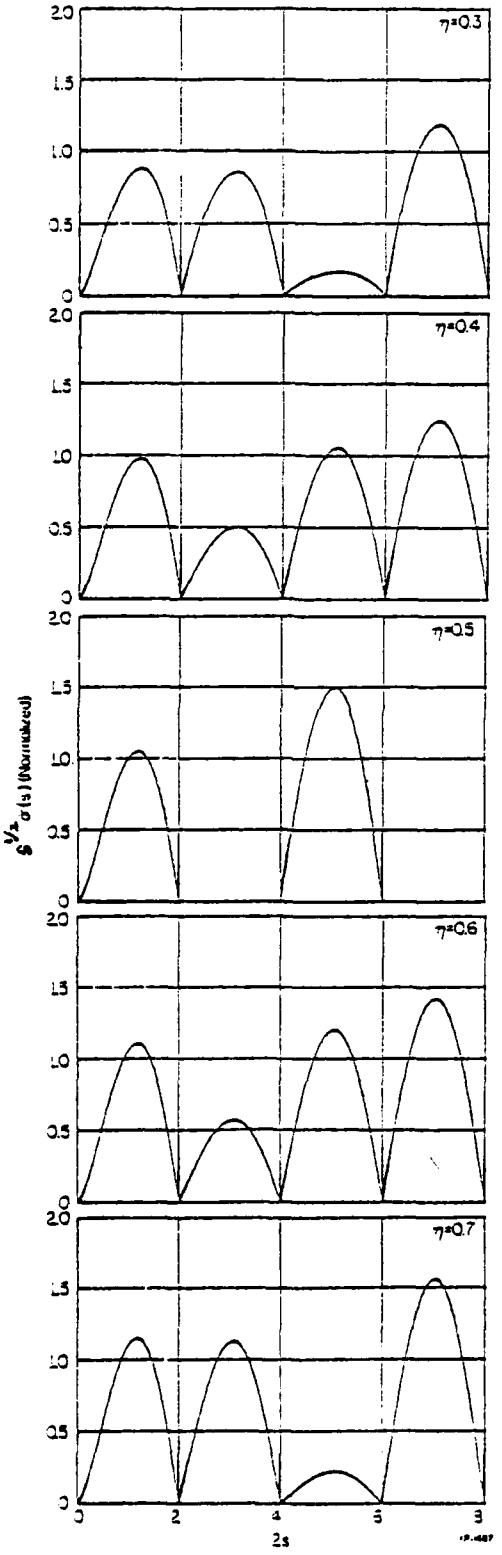

Figure 10.4: Element factor for different metalization ratios computed analytically

References

1. L. A. Coldren and R. L. Rosenberg, "SAW Resonator Filter Overview: Design and Performance Tradeoffs," IEEE Ultrasonics Symposium 1978.

2. S. Datta and B. J. Hunsinger, "Analysis of Surface Waves using Orthogonal Functions," J. Appl. Phys., Feb. 1978.

3. S. Datta and B. J. Hunsinger, "Analysis of Line Acoustical Waves in General Piezoelectric Crystals," Phys. Rev. B 15, Nov. 1977.

4. S. Datta, M. J. Hoskins and B. J. Hunsinger, "Line Acoustic Waves on Cleaved Edges," Appl. Phys. Lett., 1 Jan. 1978.

5. M. J. Hoskins, S. Datta and B. J. Hunsinger, "UHF Single-phase Line Acoustic Wave Transducers," Appl. Phys. Lett., 15 July 1978.

6. M. J. Hoskins, S. Datta, C. M. Panasik and B. J. Hunsinger, "Line Acoustic Waves on Cleaved Edges in $LiNbO_3$ and GaAs," IEEE Ultrasonics Symposium 1978.

7. S. Datta and B. J. Hunsinger, "Surface Acoustic Waves in Periodic Structures," J. Appl. Phys., to be published.

8. S. Datta and B. J. Hunsinger, "Reflection of Surface Acoustic Waves from Periodic Structures in Layered Media," IEEE Ultrasonics Symposium 1978.

9. S. Datta and B. J. Hunsinger, "A Simple Perturbation Theory for Propagating Waves," submitted to J. Appl. Phys.

10. S. Datta and B. J. Hunsinger, "An Analytical Theory for Piezoelectric Scattering by Periodic Arrays," submitted to J. Appl. Phys.

11. S. Datta and B. J. Hunsinger, "First-order Reflection Coefficient of Surface Acoustic Waves from Thin Strip Overlays," J. Appl. Phys., to be published.

12. S. Datta and B. J. Hunsinger, "An Analysis of Energy Storage Effects on SAW Propagation in Periodic Arrays," submitted to IEEE Trans. on Sonics and Ultrasonics.

13. S. Datta and B. J. Hunsinger, "A Model for Multitrack Non-periodic Multistrip Couplers," J. Appl. Phys., July 1978.

14. S. Datta and B. J. Hunsinger, "A Unified Theory of Transducers," unpublished.

15. S. Datta and B. J. Hunsinger, "Redefined Element Factor for Simplified IDT Design," Electron. Lett., 9 Nov. 1978.

16. B. J. Hunsinger and S. Datta, "A Generalized Model for Periodic Transducers with Arbitrary Voltages," IEEE Ultrasonics Symposium 1978.

17. S. Datta, B. J. Hunsinger, and D. C. Malocha, "A Generalized Model for Periodic Transducers with Arbitrary Voltages," IEEE Trans. on Sonics and Ultrasonics, May 1979.

18. S. Datta and B. J. Hunsinger, "Element Factor for Periodic Transducers," IEEE Trans. on Sonics and Ultrasonics, to be published.

19. W. R. Jones, J. J. Campbell and S. L. Veilleux, Final Report to AFCRL, Contract No. F19628-69-C-0132.

20. L. P. Solie, "Piezoelectric Waves on Layered Substrates," J. Appl. Phys., February 1973.

21. A. A. Maradudin, E. W. Montroll, G. H. Weiss, I. P. Ipatova, Theory of Lattice Dynamics in the Harmonic Approximation, 2nd ed. (Academic Press, New York, 1971), p. 524.

22. B. A. Auld, Acoustic Fields and Waves in Solids (Wiley, New York, 1973), Vol. II, p. 282.

23. W. L. Bond, Crystal Technology (Wiley, New York, 1976).

24. R. L. Whitman and A. Korpel, "Probing of Acoustic Surface Perturbations by Coherent Light," Appl. Optics, August 1969.

25. J. H. McFee, "Transmission and Amplification of Acoustic Waves in Piezoelectric Semiconductors," Physical Acoustics, Vol. IV, Part A, ed. by W. P. Mason (Academic Press, New York and London, 1966).

26. B. A. Auld, Acoustic Fields and Waves in Solids, Vol. II (Wiley & Sons, Inc., 1973), p. 162.

27. C. S. Hartmann, D. T. Bell and R. S. Rosenfeld, "Impulse Model Design of Acoustic Surface-Wave Filters," IEEE Trans. MTT-21 (1973).

28. C. M. Panasik and B. J. Hunsinger, "Scatter Matrix-based Transducer Model," submitted to IEEE Trans. on Sonics and Ultrasonics.

29. A. L. Lentine, S. Datta and B. J. Hunsinger, "Charge Distribution for Non-periodic Transducers Using a Circuit Model," submitted to IEEE Trans. on Sonics and Ultrasonics.

30. B. A. Auld, Acoustic Fields and Waves in Solids (Wiley, New York, 1973), Vol. II, p. 277.

Vita

Supriyo Datta was born in Dibrugarh, India in 1954. He obtained his B.Tech. degree from the Indian Institute of Technology, Kharagpur in 1975 and his M.S. degree from the University of Illinois at Urbana-Champaign in 1977.


DATE
ILME